Published in final edited form as:
Chem Res Toxicol. 2007 September ; 20(9): 1277–1290. doi:10.1021/tx7001349.

Comparison of the Cytotoxicity of the Nitroaromatic Drug Flutamide to Its Cyano Analogue in the Hepatocyte Cell Line TAMH: Evidence for Complex I Inhibition and Mitochondrial Dysfunction Using Toxicogenomic Screening

Kevin J. Coe[†], **Yankai Jia**[‡], **Han Kiat Ho**[§], **Peter Rademacher**[†], **Theo K. Bammler**[‖], **Richard P. Beyer**[‖], **Frederico M. Farin**[‖], **Libby Woodke**[⊥], **Stephen R. Plymate**[⊥,#], **Nelson Fausto**[▽], and **Sidney D. Nelson**[*,†]

Departments of Medicinal Chemistry, Environmental Health, Medicine, Pathology, University of Washington, Seattle, Washington 98195, Phillip Morris, Richmond, Virginia 23261, Centre for Molecular Medicine, Singapore 138673, and VAPSHCS, Seattle, Washington 98108

[†]Department of Medicinal Chemistry, University of Washington.

[‡]Phillip Morris.

[§]Centre for Molecular Medicine.

[‖]Department of Environmental Health, University of Washington.

[⊥]VAPSHCS.

[#]Department of Medicine, University of Washington.

[▽]Department of Pathology, University of Washington.

Abstract

Flutamide (FLU) is an antiandrogen primarily used in the treatment of metastatic prostate cancer. It is an idiosyncratic hepatotoxicant that sometimes results in severe liver toxicity. FLU possesses a nitroaromatic group, which may be a contributor to its mechanism of toxicity. A nitro to cyano analogue of FLU (CYA) was synthesized and used to test this hypothesis in the TGFα-transfected mouse hepatocyte cell line (TAMH). MTT cell viability assays and confocal microscopy showed that hepatocytes are more sensitive to cytotoxicity caused by FLU than CYA (LD_{50} 75 vs 150 μM, respectively). Despite the structural modification, the antiandrogen activity of CYA is comparable to that of FLU. Comparisons of transcriptomic changes caused by FLU with those caused by a panel of known cytotoxicants [acetaminophen, tetrafluoroethylcysteine, diquat, and rotenone (ROT)] indicated that FLU results in a temporal gene expression pattern similar to ROT, a known inhibitor of complex I of the electron transport chain. A subsequent microarray analysis comparing FLU to CYA and ROT revealed many similarities among these three compounds; however, FLU and ROT result in more substantial changes than CYA in the expression of genes associated with oxidative phosphorylation, fatty acid β-oxidation, antioxidant defense, and cell death pathways. Electron microscopy confirmed that FLU leads to mitochondrial toxicity that has some similarities to the

*To whom correspondence should be addressed..

Supporting Information Available: Spreadsheet containing the input and output of the KEGG pathway analyses of the CYA, FLU, and ROT array data. Selected KEGG pathways for glycolysis/gluconeogenesis, pyruvate metabolism, citric acid cycle, and oxidative phosphorylation. This information is available free of charge via the Internet at http://pubs.acs.org.

mitochondrial effects of ROT, but the morphologic changes caused by FLU were greater in scope with both intra- and intercellular manifestations. Biochemical studies confirmed that both ROT and FLU deplete cellular ATP levels and inhibit complex I of the electron transport chain to a greater extent than CYA. Thus, as compared to CYA, the nitroaromatic group of FLU enhances cytotoxicity to hepatocytes, likely through mechanisms involving mitochondrial dysfunction and ATP depletion that include complex I inhibition.

Introduction

Flutamide (FLU)[1] is an antiandrogen used primarily to treat prostate cancer. FLU can result in idiosyncratic hepatotoxicity, whose incidence has been reported to range from below 1% to almost 10% (1–3). Liver dysfunction often includes serum alanine aminotransferase (ALT)

[1]Abbreviations:

AAR$_3$	triple AR probasin luciferase promoter
ALT	alanine aminotransferase
AMAP	3′-hydroxyacetanilide
APAP	acetaminophen
AR	androgen receptor
ARE	androgen response element
CYA	cyano analogue of flutamide or 2-methyl-N-(4′-cyano-3′-[trifluoromethyl]phenyl)propanamide
DAVID	database for annotation, visualization, and integrated discovery
DHT	dihydrotestosterone
DIQ	diquat
ETC	electron transport chain
DMSO	dimethyl sulfoxide
FLU	flutamide
GSH	glutathione
ITS	insulin, transferrin, and selenium
IVT	in vitro transcription
LD$_{50}$	lethal concentration for 50% maximum cell viability
MTBE	methyl *tert*-butyl ether
MTT	methylthiazolyldiphenyl-tetrazolium bromide
MPT	mitochondrial permeability transition
RLU	relative luminescence units
RNS	reactive nitrogen species
ROS	reactive oxygen species
ROT	rotenone
TAMH	transforming growth factor α mouse hepatocyte cell line
TFEC	tetrafluorylethylcysteine

and bilirubin elevations, hepatic necrosis, and cholestasis (2). A FDA black box warning label was placed on FLU in 1999 due to concerns regarding its hepatotoxicity.

Typical for most idiosyncratic drug reactions, there are no animal models that reproduce the idiosyncratic hepatotoxicity caused by FLU in humans. The etiology of idiosyncratic hepatotoxicity involves multiple factors, including the formation of reactive intermediates, drug dose, immune response, inflammation, genetics, nutrition, and underlying disease states (4–7).

Drug structure is believed to be a critical determinant in precipitating toxicity. Structural modifications that replace a putative reactive moiety for a less reactive one have been used successfully to identify critical toxicophores and elucidate mechanisms of toxicity. For example, the positional isomer of acetaminophen (APAP), 3′-hydroxyacetanilide (AMAP), cannot form the reactive intermediate *N*-acetyl-*p*-benzoquinone-imine and does not display hepatotoxicity in mice, despite its ability to form protein covalent adducts (8,9). The antimalarial amodiaquine is associated with hepatitis and agranulocytosis in humans, and replacement of its 4′-hydroxyl group with fluorine prevents the formation of a quinone-imine and decreases protein covalent adduction and glutathione (GSH) depletion in human polymorphonuclear leucocytes (10). The antidiabetic troglitazone is an idiosyncratic hepatotoxicant whose unique chromane moiety has been postulated as a site for reactive metabolite formation based on troglitazone's greater in vitro cytotoxicity as compared to equimolar concentrations of its less toxic analogues, rosiglitazone and pioglitazone, which do not contain a chromane moiety (11–14). Thus, structural examination may identify structural alerts, whose participation in toxicity can be tested by comparing them to "safer" isosteric and/or isoelectronic replacements in model systems for toxicity.

A substructure of FLU is a nitroaromatic group (Chart 1) that often has been associated with toxicity due to its susceptibility to reduction that can yield reactive oxygen species (ROS), reactive nitrogen species (RNS), and/or electrophilic intermediates. Numerous drugs that bear a nitroaromatic group result in idiosyncratic toxicity, including nimesulide (liver), tolcapone (liver), nilutamide (liver and lung), and nitrofurantoin (liver and lung) (15). Nitro groups can be reduced by enzymes found in the endoplasmic reticulum and mitochondria (16). Under aerobic conditions, oxygen readily accepts the one-electron reduction product of nitroaromatics or its intermediates to generate superoxide anion and subsequent ROS and RNS. Under anaerobic conditions, the sequential reduction of a nitroaromatic group to an arylamine results in reactive intermediates, the nitroso and hydroxylamine species, which are capable of forming covalent adducts with proteins and depleting cellular GSH (17).

For example, nilutamide, a structural analogue of FLU that retains the nitroaromatic group (Chart 1), undergoes electron reduction by P450 reductase generating free radicals under aerobic conditions and protein covalent adducts under anaerobic conditions (18). Although FLU is not reduced as easily by P450 reductase (19), bicalutamide, a structural analogue of FLU, where the nitro group is replaced with a cyano group (along with other structural modifications) (Chart 1), has a far greater liver safety profile than FLU (20), providing circumstantial evidence that the nitroaromatic group of FLU contributes to its idiosyncratic hepatotoxicity.

To directly test the involvement of the nitroaromatic substructure on FLU toxicity, we have synthesized a nitro to cyano analogue of FLU [2-methyl-*N*-(4′-cyano-3′-[trifluoromethyl] phenyl)propanamide (CYA)] (Chart 1) and evaluated its effects in a mouse hepatocyte cell line derived from transgenic mice overexpressing human transforming growth factor α (TAMH) (21). This cell line was chosen due to the known limits of using cultured human primary hepatocytes or human hepatoma cell lines, such as HepG2, to explore mechanisms of drug

cytotoxicity (22,23). The TAMH line retains a stable phenotype and expresses drug-metabolizing enzymes, including CYP2E1 and CYP3A (24). Furthermore, it has previously been demonstrated to reproduce critical features of APAP hepatocellular injury (24). The TAMH cell line is more sensitive to FLU treatment than CYA, demonstrating both a time- and a concentration-dependent toxicity. In a preliminary toxicogenomic screening analysis, we used hierarchical clustering to compare the gene expression profile after FLU treatment with those of the well-characterized cytotoxicants APAP, rotenone (ROT), diquat (DIQ), and tetrafluorylethylcysteine (TFEC). We found that the transcriptional profile of FLU clustered with that of ROT. Because ROT is a potent inhibitor of complex I of the mitochondrial electron transport chain (ETC) (25), FLU was hypothesized to impair mitochondrial function in a fashion similar to ROT.

A second array experiment compared the temporal gene expression patterns of FLU, CYA, and ROT. This comparison showed that the transcriptional profile of FLU clearly had a greater resemblance to ROT in the magnitude of gene changes related to oxidative phosphorylation than that of CYA. In addition, FLU, distinct from ROT and CYA, more profoundly down-regulated genes related to fatty acid *β*-oxidation and upregulated genes related to antioxidant defense. On the basis of electron microscopy studies, FLU also alters the morphology of the mitochondria, implicating it as a target in cytotoxicity caused by FLU. Furthermore, FLU depletes cellular ATP and inhibits complex I of the ETC to a greater extent than CYA. Thus, by comparison of FLU with its cyano analogue, the nitroaromatic substructure of FLU appears to contribute to hepatocellular cytotoxicity, resulting in complex I inhibition, ATP depletion, and gene and morphologic changes indicative of mitochondrial dysfunction.

Experimental Procedures

Reagents

Isobutyrl chloride, *N*,*N*-diisopropylethylamine, dexamethasone, nicotinamide, soybean trypsin inhibitor, methylthiazolyldiphenyl-tetrazolium bromide (MTT), FLU, ROT, APAP, KCN, antimycin A, decylubiquinone, methyl *tert*-butyl ether (MTBE), and NAD(H) were obtained from Sigma (St. Louis, MO). DIQ was obtained from Riedel-de-Haën (Seelze, Niedersachsen, Germany), a subsidiary of Sigma. 5-Amino-2-cyano-benzotrifluoride was obtained from TCI America (Portland, OR). Dulbecco's modified Eagle's medium/Ham's F12 was obtained from Mediatech Inc. (Herndon, VA). Insulin, transferrin, and selenium (ITS) were obtained from BD Bioscience (Bedford, MA). Gentamicin, trypsin, HEPES, Dulbecco's PBS, Trizol, and Lipofectamine Plus were obtained from Invitrogen (Carlsband, CA). Streptavidin-Alexa 647 was obtained from Molecular Probes (Eugene, OR). All reagents required to process total RNA samples for microarray analysis were supplied in the One-Cycle Target Labeling and Control Reagents kit from Affymetrix (Santa Clara, CA). NMR analysis was recorded on a Bruker AV-300 NMR, and mass spectrometry was performed on a Bruker APEX III Qe Fourier transform (ion cyclotron resonance) mass spectrometer.

Synthesis of CYA

To a solution of 0.20 g (1.07 mmol) of 4-cyano-3-trifluoromethylaniline in 10 mL of MTBE, 0.15 g (1.48 mmol) of triethylamine and 0.12 g (1.10mmol) of isobutyrl chloride were added at room temperature. The solution then was stirred overnight at reflux. The following day, the solution was cooled and washed twice with dilute HCl and then once with dilute sodium bicarbonate. The organic layer was removed and dried over Na_2SO_4 and then concentrated to 25% the original volume and diluted with hexane to yield off-white crystals that after air drying weighed 0.18 g (64%); mp 133–134 °C. ^{1}H NMR ($CDCl_3$): 1.3 ppm (6H, d, CH_3, J = 7 Hz), 2.6 ppm (1H, m, CH, J = 7Hz), 7.6 ppm (1H, s, NH), 7.8 ppm (1H, dd, aromatic 6′-H, J = 9

Hz, J = 2 Hz), 7.9 ppm (1H, d, aromatic 5′-H, J = 9 Hz), 8.1 ppm (1H, d, aromatic 2′-H, J = 2 Hz). ESI MS (*m/z*) 257.0896 (M + H), 279.0712 (M + Na).

Culture Conditions

The TAMH cell line was grown in serum-free culture conditions between passages 25 and 40 as described previously (21,24). Cells were grown in Dulbecco's modified Eagle's medium/Ham's F12 supplemented with ITS (5 mg/mL insulin, 5 mg/mL transferrin, and 5 ng/mL selenium), 100 nM dexamethasone, 10 mM nicotinamide, and 0.1% (v/v) gentamicin. Trypsin was used to passage cells at 80–90% confluence, and they were inhibited with 0.5 mg/mL soybean trypsin inhibitor before cells were plated. Cultures were maintained in a humidified incubator with 5% carbon dioxide/95% air at 37 °C. Culture conditions for the M12 AR human prostate cancer cells were described previously (26,27).

MTT Cell Viability Assay

Cells were seeded and grown to confluence on 96-well plates (approximately 10000 cells per well). Dilutions of FLU and CYA stocks were prepared in dimethyl sulfoxide (DMSO), diluted in growth media, and added to the confluent monolayer. After treatment, 50 μL of MTT dye (2.5 mg/mL in PBS) was added per well followed by 200 μL of HEPES-buffered growth media and incubated at 37 °C in the dark for 3 h. The dye was then aspirated, and 25 μL of Sorenson's buffer (0.1 M glycine and 0.1 M NaCl equilibrated to pH 10.5 with 0.1 M NaOH) and 200 μL of DMSO were added to each well. The plates were read at 560 nm using a microtiter plate reader (Molecular Devices, Sunnyvale, CA) as previously described (28). Cell viability was expressed as the percent ratio of compound treatment normalized over DMSO controls. Final DMSO concentrations of <1% were not cytotoxic to cells over the time range used.

Light Microscopy

Cells were grown in 50 cm^2 Petri dishes until confluent and treated with CYA, FLU, or DMSO vehicle for 24 h. Images of the cell monolayer were taken at 20× magnification using a Nikon Diaphot 200 light microscope at exposures between 30 and 40 s.

Promoter Activity Reporter Assays in M12 AR Human Prostate Cancer Cells

This assay was previously described (26). Briefly, transient transfections of M12 androgen receptor (AR) cells with the triple AR probasin luciferase promoter (AAR_3) (a generous gift from Dr. Matusik) and pRL-null vectors were performed using Lipofectamine Plus according to the manufacturer's protocol (Invitrogen). The AAR_3 construct is an artificial reporter containing three repeats of the rat probasin androgen response element (ARE) 1 and ARE2 regions upstream of the thymidine kinase promoter. Cells (8.6×10^4 cells/wells) were seeded in 12-well plates in RPMI medium containing 5% FBS. Each well received 1.2 μg of AAR_3, 12 μg of pRL-null vector, 6 μL of Plus reagent, and 3 μL of Lipofectamine reagent in serum-free medium. After 3 h of exposure to the Lipofectamine/DNA/Plus mixture, the medium was supplemented with 1% charcoal-stripped FBS and incubated for 24 h. For inhibitory concentration–response studies, the transfection medium was removed, and cells were treated with FLU and CYA at 100 μM and 1 μM concentrations before 100 pM dihydrotestosterone (DHT) was added 1 h later. The luciferase activity was determined using the Dual-Luciferase Reporter Assay System (Promega, Madison, WI) according to the manufacturer's protocol. Results were corrected for transfection efficiency with β-galactosidase.

RNA Isolation

For Codelink microarray experiments, cells were grown to confluence in 150 cm^2 tissue culture dishes in quadruplicate for each sample and treated with APAP (5 mM), DIQ (25 μM), FLU (75 μM), and ROT (1 μM) for 4, 8, and 24 h and with TFEC (200 μM) for 2, 4, and 6 h. For

the Affymetrix microarray experiments, cells were grown to confluence in 150 cm^2 tissue culture dishes in duplicate for each sample and treated with DMSO vehicle (0.15%), CYA (75 μM), FLU (75 μM), and ROT (1 μM) for 4, 8, and 24 h. At the end of the respective treatments for both array experiments, cells were harvested by scraping with rubber policemen. The resultant cell pellets were spun down at 200*g* and washed once with ice cold Dulbecco's PBS. Immediately, 1 mL of Trizol reagent per 10^7 cells was added. After it was vortexed, the lysate was passed through a 22G needle 10 times to ensure complete lysis. Chloroform (0.2 mL) was added to every 1 mL of cell lysate and vortexed vigorously for 15 s. The tubes were left to stand for 2–3 min before spinning at 8200*g* for 15 min at 4 °C. The aqueous phase (0.5 mL) was transferred to a fresh tube, and an equivolume of 70% ethanol was added. This resulting mix was loaded onto an RNeasy column (Qiagen, Valencia, CA), and purified total RNAs were eluted in sterile water according to the manufacturer's protocol.

Codelink Microarray Gene Expression

For the preliminary toxicogenomic screening, gene expression analyses were performed using the Amersham "Codelink" 10K mouse array (Amersham Biosciences, Piscataway, NJ) according to the manufacturer's protocols. Briefly, total RNA from each sample was quantified before first and second strand cDNA synthesis. The resulting double-stranded cDNA was purified with a QIAquick spin column (Qiagen). After the cDNA was dried in a SpeedVac concentrator, cRNA was synthesized by in vitro transcription (IVT) and purified using the RNeasy kit. The quality of the cRNA was evaluated using an Agilent 2100 Bioanalyzer (Agilent, Palo Alto, CA), and only those samples with *A*260:*A*280 ratios between 1.8 and 2.1 were used for subsequent microarray analysis. Each 10 μg of cRNA sample was hybridized onto Codelink microarray slides and incubated for 18 h at 37 °C. At the end of incubation, the arrays were washed with 0.753 TNT buffer (0.1 M Tris-HCl, pH 7.6, 0.15 M NaCl, and 0.05% Tween-20) at 46 °C for 1 h and incubated with streptavidin-Alexa 647 working solution at 25 °C for 30 min to label the fluorogenic probe. The arrays were scanned with an Axon GenePix 4000B fluorescent scanner and the GenePix Pro imaging software (Axon Instruments, Foster City, CA). The fluorescent intensity of each spot in the image was determined using ImaGeneTM 5 (Biodiscovery, Marina del Rey, CA) for spot finding and analysis.

Affymetrix Microarray Gene Expression

RNA quality was assessed with an Agilent 2100 Bioanalyzer, and only samples passing QC were further processed. The manufacturer's protocols were followed for the technical aspects associated with the determination of gene expression using the Affymetrix Mouse Genome 430 2.0 array (Santa Clara, CA) providing genome wide coverage. These methods include the synthesis of first- and second-strand cDNAs, the purification of double-stranded cDNA, the synthesis of cRNA by IVT, the recovery and quantitation of biotinlabeled cRNA, the fragmentation of this cRNA and subsequent hybridization to the microarray slide, the posthybridization washings, and the detection of the hybridized cRNAs using streptavidin-coupled fluoresecent dye. Hybridized Affymetrix arrays were scanned with an Affymetrix GeneChip 3000 scanner. Image generation and feature extraction were performed using Affymetrix GCOS Software. Only data from arrays that passed the manufacturer's quality specifications with respect to background and percent present call rates were used for further analysis.

Statistical Analysis and Data Normalization

Statistical analyses and data normalization were carried out with Bioconductor software (29). The foreground mean spot intensities from all the Codelink microarrays used were normalized as a group using quantile normalization as described previously (30). Raw microarray data from the Affymetrix arrays were also processed and analyzed with Bioconductor and

normalized with the Bioconductor gcrma package (31). Following data normalization, genes with significant evidence of differential expression were identified using the Bioconductor limma package (32). Differential gene expression results from both CodeLink arrays and Affymetrix GeneChip arrays were compared by cross-referencing the two platforms using the TIGR Resourcerer software (33), which is a database built using expressed sequence tags and gene sequences provided by the TIGR Gene Index and TIGR Orthologous Gene Alignment databases.

Pathway Analysis and Gene Extraction

Gene probes regulated ≥2-fold (a $\log_2$ value of ≥1) were considered significantly regulated probes and were extracted from each individual sample treatments of 4, 8, and 24 h. Gene probes found significantly regulated for at least one time point employed were pooled for each compound (CYA, FLU, or ROT) and divided between up- and down-regulated probes for subsequent gene and pathway analysis. Gene and pathway analysis utilized the web-accessible program DAVID [Database for Annotation, Visualization, and Integrated Discovery (http://david.abcc.ncifcrf.gov/)] that conveniently permits input of long lists of Affymetrix probe IDs and output of gene function and pathway mapping information that integrates annotation data from commonly used resources such as GenBank (http://www.ncbi.nlm.nih.gov/Genbank/GenbankSearch.html), Gene Ontology (http://www.geneontology.org/), and KEGG (http://www.genome.ad.jp/kegg/) among others (34). For KEGG pathway analysis on DAVID, each compound set of up- and down-regulated gene probes was input separately to identify significant pathways that consisted of at least two gene members and had an EASE statistical value of <0.5. The EASE tool helps “identify statistically over-represented functional categories within a given list of genes” (34,35). Further gene probes were extracted by mining the complete Affymetrix data set using KEGG nomenclature for metabolism-related pathways such as oxidative phosphorylation, glycolysis, citric acid cycle, etc. and GO nomenclature for mitochondrion-related gene probes.

Electron Microscopy Analysis

Adherent hepatocytes from DMSO vehicle (0.15%), CYA (75 μM), FLU (75 μM), and ROT (1 μM) remaining after 24 h of treatment were trypsinized from the monolayer. The resulting cell pellet after soybean trypsin inhibition was gently resuspended in Karnovsky’s fixative (one-half strength glutaraldehyde-formaldehyde) and chilled overnight at 4 °C. Cells were rinsed twice in 0.1 M phosphate buffer for 10 min each before postfixing in 1% osmium tetroxide in phosphate buffer for 1.5 h at room temperature. Following two additional 10 min rinses in phosphate buffer, the cells were dehydrated in an ascending ethanol gradient (50, 70, 90, and 100%) for 10 min each and rinsed in propylene oxide three times for 10 min each. Cells were mixed in a 1:1 ratio of propylene oxide:resin for 1.5 h on a rotary shaker and remixed for an additional 2 h in resin alone. Specimens were placed in embedded capsules and polymerized at 60 °C overnight and later examined using a Phillips 410 transmission electron microscope. Without knowledge of the anticipated sample outcome, the spectroscopist was instructed to take snapshots of cell clusters where mitochondria were apparent for each specimen.

ATP Depletion Assay

The intracellular ATP level was measured by its activity using the CellTiter-Glo Luminescent Cell Viability Assay (Promega) according to the manufacturer’s protocol. Briefly, cells were treated with FLU, CYA, and ROT on 96-well plates. After incubation for 2 h, an equivolume of the luminescent substrate and lysis buffer mix from the assay kit was supplied. The mixture was transferred to an opaque 96-well plate, and luminescence was read and analyzed with PlateLumino (Phenix, Hayward, CA).

Mitochondrial Isolation and Complex I Inhibition Assay

Cells were grown to confluence on 20 150 cm^2 Petri dishes (~1×10^7 cells/dish), scraped using a cell scraper, and centrifuged at 200*g* using a benchtop centrifuge. Mitochondria from the cell pellet were isolated by following the methods of the Sigma Mitochondrial Isolation Kit (Sigma) and stored at −70 °C until use. The protein concentration was determined by the BCA protein assay kit (Pierce, Rockford, IL), where albumin served as the standard.

The complex I activity was measured using the procedure of Birch-Machin et al. (36), except that decylubiquinone was used in place of ubiquinone. Briefly, ethanol stock concentrations of FLU (5 mM), CYA (5 mM), and ROT (25 μM) were diluted to working concentrations in a complex I buffer (50 mM potassium phosphate, pH 7.4, supplemented with 10 mM $MgCl_2$, 5 mg/mL bovine serum albumin, 2.1 mM KCN, 2 μg/mL antimycin A, and 130 μM decylubiquinone). Antimycin A (400 μg/mL) and decylubiquinone (10 mM) were supplemented as ethanol stock concentrations. Mitochondria (20 μg) were added to the buffer, and reactions were initiated with the addition of NAD(H) (130 μM) prepared from a 2 mM stock concentration in 0.01 N NaOH. Reactions were allowed to equilibriate at 30 °C for 3 min before the depletion of NAD(H) was monitored spectrally at 340 nm for 3 min by a CARY 3E UV–visible spectrophotometer (Varian Inc.) counterbalanced with a blank absent of NAD(H). The complex I activity rate is expressed as the nmol of NAD(H) consumed per minute per mg of mitochondrial protein at 340 nm $\varepsilon = 6200\ M^{-1}\ cm^{-1}$). The complex I percent activity is expressed as the percent ratio of inhibitor over vehicle treatment rates.

Results

Comparison of the Cytotoxicity and Antiandrogen Activity of FLU to CYA

Various concentrations of the nitroaromatic drug FLU were tested over time in the TAMH cell line to evaluate cytotoxicity using the MTT cell viability assay. At concentrations of 50 μM and greater, FLU demonstrated both a time- and a concentration-dependent toxicity with a lethal concentration for 50% maximum cell viability (LD_{50}) of ~75 μM after 24 h of exposure (Figure 1A). Although DMSO can alter CYP activity and expression (37, 38), varying DMSO concentrations did not affect FLU-mediated cytotoxicity. To test the hypothesis that the nitroaromatic group of FLU is a contributor to its cytotoxicity, CYA, the cyano analogue of FLU, was tested at equimolar concentrations for 24 h. From the summation of three biological replicates, the TAMH cell line is more sensitive to FLU than to CYA across all concentrations tested with $p < 0.01$ for concentrations from 75 to 200 μM and $p < 0.05$ for the 50 μM concentration (Figure 1B). At the LD_{50} value of 75 μM for FLU, CYA-treated cells retain ~90% viability and require concentrations of ~150 μM to achieve its LD_{50} value, which is approximately 2-fold greater than that of FLU. Confocal light microscopy analysis was consistent with the MTT cell viability assays, displaying an impairment of cell–cell adhesion, a disruption of the cell monolayer, and an elevated number of detached cells (white globules) with increasing concentrations of FLU from 75 to 200 μM (Figure 1C). Hepatocyte cell swelling, indicative of oncosis, was apparent in cells (panel d) after 24 h of treatment with 100 μM FLU. In contrast, equimolar concentrations of 75 and 100 μM CYA (panels a and b, respectively) retained cell–cell attachments and a confluent monolayer and had cell morphologies similar to vehicle-treated hepatocytes (panel e).

Because the change from a nitro group to a cyano group may alter FLU vs CYA binding to the AR, luciferase reporter assays were employed to test the ability of CYA to antagonize the binding of the agonist DHT as compared to FLU in the M12 AR cell line. At a concentration of 100 μM, both FLU and CYA antagonize DHT stimulation similarly with the notable exception that CYA causes ~3-fold less partial agonist effect than FLU (Figure 2), an effect noted for FLU elsewhere (39). At a concentration of 1 μM, both FLU and CYA do not

antagonize DHT. Thus, FLU and CYA have comparable antiandrogen activities. Overall, CYA was less cytotoxic than FLU in the TAMH cell line yet still capable of antagonizing the AR to a similar extent as FLU.

Toxicogenomic Screening of FLU and Other Known Hepatotoxicants

To gain further mechanistic insight concerning cytotoxicity caused by FLU, temporal gene expression profiles were generated, using the Amersham "Codelink" microarray with 10000 genes, for FLU and the toxicants APAP, DIQ, ROT, and TFEC whose mechanisms of toxicity are better understood. Because each sample was performed as a single array replicate, statistical *p* values could not be assigned, and instead, a gene-fold cutoff of >2 was used to identify meaningful gene expression changes. Genes whose expression was changed more than 2-fold by at least one of the toxicant treatments (2031 probes in total) were selected for two-dimensional hierarchical cluster analysis to generate a dendrogram (Figure 3). Both FLU 4 and 8 h treatments are adjacent to 4 and 8 h ROT treatments, and after 24 h of treatment, both cytotoxicants are clustered together, suggesting that FLU and ROT bear a similar temporal pattern of gene expression that is distinct from the other cytotoxicants APAP, DIQ, and TFEC. Because toxicants alter gene expression in relationship to their mechanism of toxicity, toxicants that bear a similar route of toxicity generally have similar patterns of gene expression, ultimately allowing for array analysis to serve as a predictive tool for unknown toxicants as compared to established toxicants (40). Thus, FLU may cause cytotoxicity in the TAMH cell line in a fashion comparable to that of ROT, a known inhibitor of complex I of the ETC (25).

Array Comparison of FLU to CYA and ROT

To differentiate cytotoxicity caused by FLU from its less toxic analogue, a second microarray experiment compared the gene expression profiles of FLU (75 μM) to CYA (75 μM) and ROT (1 μM) across 4, 8, and 24 h using the Affymetrix array platform, which, in contrast to the Amersham Codelink platform, provides whole genome coverage. Because microarray gene responses can vary between platforms and experiments, common gene probes were identified between the two platforms, and their expression profiles for FLU and ROT were compared (Figure 4). The majority of gene probes mapped along or near a slope of 1 (the diagonal 45° axis), especially for the earlier 4 and 8 h time points, indicating that gene response was comparable between the platforms. At 24 h, both ROT and FLU gene responses diverged more from this axis than earlier time points, although they clearly retained a positive slope. This might be expected considering the multitude of factors that influence the time course and magnitude of a gene's response under sustained toxic insult. In addition, it is well-established that technical differences between microarray platforms contribute to differences in results (41). Despite the aforementioned factors contributing to differences in results, the expression profiles generated by both platforms at the different time points correlated well overall and, thus, allowed for the direct array comparison of FLU to CYA.

For direct array comparison, significantly regulated gene probes with a fold change >2 are presented as a one-dimensional hierarchical clustering heat map with samples ordered according to compound treatment (Figure 5A). Prominent clades of downregulated genes (blue) and up-regulated genes (yellow) to the left and right of the heat map, respectively, indicate that all three compounds bear a strikingly similar pattern of gene expression. Over the 4, 8, and 24 h time course, 1520, 1918, and 4066 gene probes were significantly affected, respectively, by FLU, while 391, 485, and 2081 gene probes were affected by CYA. A wider range of genes affected by FLU than CYA would be anticipated considering the greater cytotoxicity of FLU than its analogue.

A dendrogram showing two-dimensional hierarchical clustering of 2-fold significant gene changes parses FLU away from CYA and ROT at the early 4 and 8 h time points but aligns

FLU with ROT at the 24 h time point (Figure 5B). One explanation for FLU's parsing from early time points of CYA and ROT is due to FLU's profound effects on early gene expression. FLU caused a greater number of gene probe regulatory changes than CYA and ROT across all time points as illustrated in the temporal Venn diagrams (Figure 5C). The time course for FLU-mediated cytotoxicity may occur earlier than that for ROT, hence explaining the greater influence that FLU has on early gene expression as compared to ROT. Nevertheless, after 24 h of exposure to LD_{50} concentrations of FLU and ROT, the gene expression patterns caused by both compounds are more similar to each other than to CYA. Furthermore, FLU and ROT have more genes commonly regulated than when either is compared to CYA (Figure 5C). Overall, the results show that FLU and ROT cause more similar cell dysregulation than CYA; however, FLU has many unique gene changes, especially at early time points, suggesting that it causes additional effects beyond effects caused by ROT and beyond its pharmacological effects that are in common with CYA.

To deconvolute the complexity inherent in array data, KEGG pathway analysis using the web-accessible software tool DAVID (34) was employed using a summation of gene probes found either up- or down-regulated across the three time points (depicted in Figure 5C) for each compound. The full KEGG pathway output is provided in the Supporting Information, and selected pathways related to carbohydrate and fatty acid energy metabolism and cell cycle are presented (Figure 6). Genes regulated by FLU, CYA, and ROT, or by all three compounds [the union of the three compounds displayed in the Venn diagrams (Figure 5C)] were assessed for their ability to statistically perturb a KEGG pathway using up-regulated genes (orange box) or down-regulated genes (cyan box). KEGG pathways statistically perturbed by the input of both up- and down-regulated genes are depicted as green boxes, and nonresponsive KEGG pathways are blackened. Notably, for genes found in common for all compounds, up-regulated genes perturb pathways related to carbohydrate metabolism, including glycolysis, and down-regulated genes perturb pathways involved in glycosylation. The glycolysis pathway is perturbed by both CYA and ROT up-regulated genes but not for FLU, despite the observation that up-regulated genes found in common for all three compounds perturb this pathway. Because the EASE tool identifies perturbed KEGG pathways statistically based upon the enrichment of genes associated with a particular pathway in relation to the overall gene input, the apparent inability of FLU to perturb this pathway may be due to its larger gene input as compared to CYA and ROT, which dampens effects on glycolytic-related genes in relationship to the overall gene input. For the FLU gene set, down-regulated genes perturb pathways related to fatty acid elongation and metabolism that are not affected by the CYA and ROT gene sets.

Genes extracted from the KEGG analysis and other genes that code for proteins involved in energy metabolism, mitochondrial processes, and cellular stress are presented in Table 1. KEGG analysis (Figure 6) suggests that FLU results in greater down-regulation of genes associated with fatty acid metabolism. Genes related to long chain fatty acid activation (*Acsl1* and *Acsl2*), transport (*Cpt1a*, *Slc25a20*, and *Cpt2*), and utilization in *β*-oxidation (*Acadl*, *Ehhadh*, *Hadha*, and *Hadhb*) are down-regulated to a greater extent by FLU than by either CYA or ROT, which trend similarly downward. KEGG analysis also suggests that all compounds up-regulate genes related to carbohydrate metabolism. Up-regulation of genes related to the initial steps of glycolysis (*Hk1*, *Hk2*, *Gpi1*, and *Aldoa*) and to carbohydrate utilization (*Galm*, *Gla*, *Hexa*, and *Cyb5r1*) are apparent for all compounds, supporting the KEGG results; however, down-regulation of other glycolytic and citric acid cycle genes indicates a complicated gene response that does not clearly provide insight into the metabolic outcome after compound treatment. ROT clearly alters gene expression of subunits involved in the assembly of various complexes of the ETC, including I, III, IV, and V. Gene trends are similar for FLU and CYA; however, FLU more closely resembles the magnitude of ROT gene responses for most genes. Notably, all compounds up-regulate the cell stress sensitive genes *Atf3* and *Gadd45a*; however, FLU and ROT show greater effects on genes affected by cell

stress. The mitochondrial stress-related genes (*Bax*, *Pmaip1*, and *Grpel2*) are up-regulated for FLU and ROT, and the antioxidant stress response genes (*Gsta2*, *Ugt1a6*, *Gclc*, *Hmox1*, *Gsr*, and *Txn2*) are particularly responsive to FLU treatment as compared to CYA and ROT.

Electron Microscopy Analysis Suggests that FLU Induces Mitochondrial Dysfunction

To relate array observations to alterations in cellular morphology, electron microscopy studies of cells with abundant and observable mitochondria after exposure to compounds for 24 h are presented (Figure 7). Both DMSO vehicle- (0.15%) and ROT- (1 μM) treated TAMH cells had a uniform overall mitochondrial morphology both inter- and intracellularly. However, mitochondria in vehicle-treated cells have visible cristae folds in contrast to ROT-exposed mitochondria, which are clearly vacuous with the cristae remnants either fragmented or dilated and, occasionally, contain calcium phosphate crystal inclusions (denoted by black arrowheads). In contrast to vehicle and ROT, FLU and CYA at 75 μM resulted in a mixed mitochondrial morphology that differs both inter- and intracellularly illustrated by two cell snapshots for each compound. In FLU 1, the cell's mitochondria all have an increased electron density of the cristae folds in the matrix. Interestingly, for a different cell (FLU 2), the same electrondense mitochondria observed in FLU 1 are found adjacent to swollen vacuous mitochondria, where cristae remnants are granulated and fragmented throughout the mitochondria. Phagolysosomes (P) are also prominent in FLU 2. CYA-treated cells have a mitochondrial morphology that is significantly less severe in appearance than FLU-treated cells. In CYA 1, mitochondria have greater electron density within the matrix than vehicle-treated cells but not to the same extent as found in FLU-treated cells. In CYA 2, a different morphology than CYA 1 is observed, where mitochondria appear swollen and the cristae are more dilated as compared to vehicle and CYA 1. The mitochondrial morphology in CYA 2 (the worst identified) still lacked the bloated, vacuous morphology of FLU 2, where the cristae folds are clearly no longer intact. Thus, the electron microscopy analysis supports the hypothesis that the mitochondrion is a target organelle for FLU-mediated cytotoxicity.

Comparison of ATP Depletion between FLU, CYA, and ROT

Because one possible consequence of mitochondrial dysfunction is a loss of ATP generation via oxidative phosphorylation, ATP levels were compared among cells treated with FLU, CYA, and ROT. A marked decline in ATP levels occurs after 2 h of FLU treatment (up to 85% at 100 μM FLU), and this parallels with the increased cytotoxicity (Figure 8A). In contrast, similar concentrations of CYA cause minimal cytotoxicity and only modest declines in cellular ATP.

Interestingly, a comparison of ATP levels at the LD_{50} concentration of FLU and ROT after 2 h of treatment reveals that, despite the equivalent extent of cytotoxicity after 24 h, FLU results in a 2-fold greater decline in ATP than ROT ($p < 0.05$) (Figure 8B). Thus, FLU is more capable of depleting ATP than ROT at an equitoxic concentration, although the time course of toxicity after 2 h of treatment may differ between the two cytotoxicants. ATP levels appear to be a critical element in the cytotoxicity caused by FLU, since TAMH cells grown in media without glucose demonstrate a greater sensitivity to FLU-mediated cytotoxicity and ATP depletion than cells grown in high glucose media (data not shown).

Complex I Inhibition

The rapid ATP depletion caused by FLU and similar gene expression to ROT suggested that complex I of the ETC was a target in the mechanism of toxicity caused by FLU. Complex I activity assays that monitored the depletion of NAD(H) over time using mitochondrial isolates from the TAMH cells were used to evaluate the inhibitory capabilities of FLU, CYA, and ROT. FLU displayed a concentration-dependent inhibition of complex I activity with an IC_{50} of ~150 μM (Figure 9). CYA also demonstrated complex I inhibition, although at significantly higher concentrations than FLU ($p < 0.01$).

A comparison of FLU and ROT complex I inhibition reveals that ROT is a more potent inhibitor of complex I than FLU. Using the LD_{50} concentrations of ROT (1 μM) and FLU (75 μM), ROT reduces the rate of complex I to 13% of the control as compared to 69% of control activity for FLU. Thus, despite an equivalent toxic end point in the TAMH cell line, ROT is a more potent inhibitor of complex I than FLU, suggesting that additional factors beyond complex I inhibition contribute to the cytotoxicity caused by FLU.

Discussion

Idiosyncratic drug reactions represent a significant challenge for health care and drug development, since they often go undetected in early clinical trials and only manifest when the drug has reached the market (42). Screening methods to eliminate idiosyncratic drugs are hampered due to the multifactor etiology of idiosyncratic reactions that involve the complex interplay of patient genetics, nutrition, disease state, and other environmental factors. As such, mechanistic information regarding a drug's role in causing idiosyncratic drug reactions remains poorly understood. Evaluation of a drug's ability to cause cytotoxicity in hepatocytes represents one means of studying idiosyncratic hepatotoxicants, especially when no animal model exists. However, such studies, which often require higher concentrations to achieve cytotoxicity than otherwise found clinically, should not be considered reproductions of the complex human event and are often considered an evaluation of a drug's intrinsic toxicity (43). Nevertheless, hepatocytes represent a convenient model to evaluate a drug's ability to cause cytotoxicity (44) and can provide informative mechanistic information that may aid in understanding a drug's role in contributing to idiosyncratic drug reactions. Furthermore, hepatocytes represent a simple model system to evaluate the contribution certain substructures, such as the nitroaromatic group, have on cytotoxicity ascomparedto "safer" isosteric/isoelectronic replacements.

Considering the association of nitroaromatic drugs with idiosyncratic toxicity, the contribution of the nitroaromatic group of FLU to cytotoxicity was assessed by comparing effects of its cyano analogue in (i) cytotoxicity assays in the TAMH hepatocyte cell line, (ii) transcriptomic studies, (iii) electron microscopic morphological studies, and (iv) biochemical assays.

In hopes of decreasing the inherent cytotoxic potential of FLU, while preserving its antiandrogen activity, the cyano analogue of FLU, CYA, was synthesized. The nitro to cyano replacement prevents the possibility of reduction of the nitroaromatic group, eliminating a potential route of cytotoxicity, while retaining a strong electron-withdrawing group at the para position that may preserve drug efficacy. In fact, in M12 AR cells, CYA had antiandrogen activity essentially equivalent to that of FLU. With respect to cytotoxicity, in the TAMH hepatocyte cell line, FLU caused greater cytotoxicity than CYA with an approximate 2-fold difference in the LD_{50} value after 24 h (~75 and ~150 μM, respectively).

Toxicogenomic profiling of FLU as compared to known cytotoxicants identified impairment of mitochondrial function, perhaps of oxidative phosphorylation, as one explanation for its cytotoxicity. FLU has been found to be an ETC inhibitor of complex I and to a lesser extent of complex III that resulted in ATP depletion in rat hepatocytes (45). Therefore, gene profiles of different toxicants (APAP, DIQ, ROT, and TFEC), whose mechanisms of toxicity are fairly well understood, were used to help identify features of the cytotoxicity caused by FLU. The cytotoxicity of ROT, DIQ, and TFEC originates within the mitochondrion: ROT is a potent inhibitor of complex I that inhibits the ETC (25); DIQ is capable of futile cycling within the mitochondria that results in oxidative stress (46); and TFEC is bioactivated in the mitochondria resulting in covalent adduction to adjacent mitochondrial proteins, including heat shock proteins and citric acid cycle enzymes (47). APAP results in downstream mitochondrial toxicity through GSH depletion and protein covalent adduction after sufficient P450

bioactivation leads to depletion of cytosolic GSH stores (48–50). Temporal gene expression changes caused by FLU as compared to effects of these cytotoxicants revealed that FLU generated a similar gene expression pattern to that of ROT, and this pattern was different from the other cytotoxicants. This provided preliminary support that FLU elicits cytotoxicity through a mechanism similar to ROT, perhaps by inhibiting mitochondrial oxidative phosphorylation.

The direct array comparison of FLU to CYA identified transcriptional profiles that were shared among FLU, CYA, and ROT. However, certain gene expression changes were only associated with FLU treatment, especially at early time points, and suggests that FLU causes additional cellular effects unrelated to its putative effects on oxidative phosphorylation (as observed with ROT) and unrelated to its pharmacology (as observed with CYA).

KEGG pathway analysis suggested that FLU promotes down-regulation of genes associated with fatty acid metabolism. Long chain fatty acids are made available for *β*-oxidation in mitochondria through a sequential process that involves formation of acyl-CoA thioesters mediated by acyl-CoA synthetase, coupling with L-carnitine by carnitine palmitoyltransferase 1, transport into the matrix of mitochondria by Slc25a20 (a.k.a. mitochondrial carnitine/acylcarnitine translocase), and release of L-carnitine by carnitine palmitoyltransferase 2. Isoforms of these genes are all down-regulated to a greater extent by FLU than by either CYA or ROT. Furthermore, FLU results in a greater down-regulation of genes involved in *β*-oxidation, including the long and medium chain acyl-CoA dehydrogenases and subunits of the trifunctional enzyme Hadh, which in summation, account for all of the enzymatic reactions necessary for one cycle of *β*-oxidation. Although it remains unclear to what extent FLU is perturbing the flux of this pathway, it may be doing so through an indirect mechanism, as has been observed for ROT and nilutamide (51), which are believed to slow *β*-oxidation rates through complex I inhibition, which in turn depletes mitochondria of available NAD+ required for *β*-oxidation. Thus, similar to its nitroaromatic structural analogue nilutamide and to its array comparator ROT, FLU may also be causing a decreased flux in *β*-oxidation, an effect anticipated to be greater than that caused by CYA and ROT based on the magnitude of gene responses.

KEGG pathway analysis also demonstrated a perturbation of glycolysis/gluconeogenesis-related genes by all compounds. These up-regulated genes are associated with hexose sugar availability and with early glycolytic enzymes, including hexokinases, glucose phosphate isomerase, and aldolase b. Although our array analysis shows up-regulation of hexokinase 1 after FLU and ROT treatments and of hexokinase 2 after treatment with all compounds, phosphofructokinase is down-regulated after both CYA and ROT treatment, and pyruvate kinase is down-regulated after FLU treatment. The mixed transcriptional changes of these allosterically regulated enzymes confound speculation on the flux of glycolysis. Allosteric regulation of these pivotal enzymes may be more crucial to the flux of glycolysis than their transcriptional changes. As such, assessment of metabolic end points, such as lactate, may serve as a better marker than transcriptional changes to gauge the impact that the three compounds have upon glycolysis. Nevertheless, glycolysis appears to be the primary route of energy generation in FLU-treated cells, since FLU-mediated cytotoxicty and ATP depletion were significantly greater in media absent in glucose as compared to media high in glucose.

Two pathways not uncovered by the KEGG pathway analysis that are probably relevant to this study, considering the known mechanism of toxicity caused by ROT, are oxidative phosphorylation and cell stress. ROT and FLU caused similar responses for regulated gene probes of oxidative phosphorylation, including subunits associated with complexes I, III, IV, and V. All complex subunits are up-regulated except for complex I, the primary target of ROT toxicity, which displayed a mixed response of both up- and down-regulated genes. Importantly, FLU caused a greater fold change than CYA for most of the genes in this subset; however,

CYA certainly did cause similar trends in gene expression, suggesting that CYA also alters oxidative phosphorylation.

All compounds up-regulated the cell stress sensitive genes *Atf3* and *Gadd45a*. Correlating with its greater cytotoxicity, FLU causes a greater fold change of these genes than CYA. Interestingly, both FLU and ROT, distinct from CYA, up-regulate *Bax* and *Pmaip1* (a.k.a. *Noxa*), two genes known to modulate the mitochondrial permeability transition (MPT) and promote release of cytochrome *c* (52,53). These marker genes suggest that FLU and ROT promote mitochondrial dysfunction to a greater extent than CYA. The up-regulation of the mitochondrial hexokinases 1 and 2 bolsters this conclusion, as these glycolytic enzymes have been shown to have additional cytoprotective roles in preventing the opening of the mitochondrial voltage dependent anion channel (54).

Finally, FLU, distinct from CYA and ROT, results in greater up-regulation of genes responsive to the oxidative stress "sensing" transcription factor Nrf2, including *Gsta2*, *Gclc*, *Hmox1*, and *Txn2*. This gene battery is up-regulated collectively as a cytoprotective response to combat oxidative stress induced by various triggers, including drug-induced oxidative stress (55). Metabolism of FLU into electrophilic intermediates or through redox cycling may cause cellular oxidative stress capable of activating Nrf2. Metabolism studies of FLU in hepatocytes and microsomes have previously shown P450-mediated metabolism of FLU capable of forming reactive metabolites that covalently adduct protein and GSH (45,56–58). An in vivo genomic study in rodents has also demonstrated that FLU is capable of up-regulating Nrf2 associated genes, including *Gclc*, *Glrx1*, *Gsr*, *Gsta2*, *Hmox1*, *Nqo1*, and *Ugt1a6* (59). ROT has been demonstrated to have a mixed influence on ROS generation (53,60,61), which may explain its limited impact upon Nrf2-regulated genes in the TAMH cell line. Thus, the activation of antioxidant response-associated genes by FLU, and less so by ROT, suggests that FLU may have some mechanisms that modulate toxicity differently from ROT.

These observations, with respect to FLU and ROT, correlate with the electron microscopy and biochemical data. Although each toxicant clearly elicits mitochondrial toxicity at an equitoxic end point, their manifestations are distinguishable, suggesting that FLU does not solely cause toxicity through complex I inhibition (as does ROT). The mitochondrial morphology observed in TAMH cells exposed to FLU or ROT are quite distinct, both inter- and intracellularly. ROT, known to induce MPT (62), results in vacuous mitochondria with cristae barely intact in the TAMH cell line. Unlike these uniform changes, cells exposed to FLU either have electron dense or visibly swollen, vacuous mitochondria, and in some cases, both kinds of changes occur in the same cell. Additionally, a comparison using LD_{50} concentrations of FLU and ROT shows that FLU causes a greater ATP depletion than ROT after 2 h of treatment, but that ROT is a more effective inhibitor of complex I. Overall, array, electron microscopy, and biochemical evidence suggest that FLU has at least some mechanisms of toxicity that are different from those of ROT.

With respect to FLU and CYA, although less toxic, the mechanism of CYA cytotoxicity is apparently similar to that of FLU in some ways. Although significantly higher concentrations than FLU are required, CYA results in a concentration-dependent loss of cell viability and ATP stores, alters some genes and gene-associated pathways similar to FLU, perturbs mitochondrial morphology, and inhibits complex I activity. Thus, despite the removal of the nitro group of FLU, CYA appears to work as a less potent mitochondrial toxicant than FLU. Redox cycling of the nitro group of FLU may explain the additional mechanism that distinguishes FLU from its less toxic analogue CYA, perhaps in a fashion similar to the complex I inhibitor doxorubicin (63); however, this remains to be demonstrated. Alternatively, the nitro group may simply allow for a greater binding affinity than its cyano analogue to the target(s) relevant to FLU-

mediated cytotoxicity. As such, the chemotype shared by FLU and CYA may be a cause for the cytotoxicity elicited.

FLU has been demonstrated to form reactive metabolites that do not involve nitro group reduction (56–58,64). It is conceivable that CYA is metabolized to similar reactive metabolites at slower rates. Additional studies comparing the metabolism of FLU and CYA in the TAMH cell line are underway.

In conclusion, the replacement of the nitroaromatic substructure of FLU with a cyano aromatic group improves its cytotoxicity profile in the TAMH hepatocyte cell line without loss of pharmacological activity. As compared to CYA, FLU causes greater cytotoxicity, gene expression changes suggestive of cellular toxicity, morphology indicative of mitochondrial dysfunction, ATP depletion, and ETC complex I inhibition. This difference may be due to reduction of the nitro group of FLU, but alternative explanations, such as binding affinity to target(s) related to toxicity or differences in P450 metabolism, cannot be ruled out. The mitochondrion certainly represents a target organelle associated with FLU cytotoxicity. Despite a similar pattern of gene expression, especially across oxidative phosphorylation and mitochondrial -related genes, FLU does not identically reproduce the cytotoxicity caused by ROT, as ROT results in a uniform alteration in mitochondrial morphology and a greater extent of complex I inhibition at an equitoxic concentration. Intriguingly, FLU results in a greater induction of Nrf2 responsive genes distinct from ROT and CYA, indicating that FLU causes cellular oxidative stress as part of its mechanism of toxicity. Future work on the metabolism of FLU and its relationship to oxidative stress and impairment of mitochondrial function is necessary to further relate the structural liability of the nitroaromatic substructure to cytotoxicity mechanisms.

Supplementary Material

Refer to Web version on PubMed Central for supplementary material.

Acknowledgments

This work was funded by Amgen, Pfizer Inc., the UW NIEHS sponsored Center for Ecogenetics and Environmental Health (Grant NIEHS P30ES07033), and the NIH Training Grant Drug Action, Metabolism, and Kinetics GM07750. We also thank Holly Predd and Chiyen Miller (Department of Anatomic Pathology, University of Washington) for their preparation of our electron microscopy slides and Dr. Terry Kavanagh (Department of Environmental Health, University of Washington) and Dr. David Hockenbery (Fred Hutchinson Cancer Research Center) for their expertise in examining them.

References

(1). Cortes, M. Garcia; Andrade, RJ.; Lucena, MI.; Martinez, H. Sanchez; Fernandez, MC.; Ferrer, T.; Martin-Vivaldi, R.; Pelaez, G.; Suarez, F.; Romero-Gomez, M.; Montero, JL.; Fraga, E.; Camargo, R.; Alcantara, R.; Pizarro, MA.; Garcia-Ruiz, E.; Rosemary-Gomez, M. Flutamide-induced hepatotoxicity: report of a case series. Rev. Esp. Enferm. Dig 2001;93:423–432. [PubMed: 11685939]

(2). Gomez JL, Dupont A, Cusan L, Tremblay M, Suburu R, Lemay M, Labrie F. Incidence of liver toxicity associated with the use of flutamide in prostate cancer patients. Am. J. Med 1992;92:465–470. [PubMed: 1349790]

(3). Wysowski DK, Fourcroy JL. Flutamide hepatotoxicity. J. Urol 1996;155:209–212. [PubMed: 7490837]

(4). Boelsterli UA. Disease-related determinants of susceptibility to drug-induced idiosyncratic hepatotoxicity. Curr. Opin. Drug Discovery Dev 2003;6:81–91.

(5). Li AP. A review of the common properties of drugs with idiosyncratic hepatotoxicity and the "multiple determinant hypothesis" for the manifestation of idiosyncratic drug toxicity. Chem.-Biol. Interact 2002;142:7–23. [PubMed: 12399152]

(6). Roth RA, Luyendyk JP, Maddox JF, Ganey PE. Inflammation and drug idiosyncrasy--is there a connection? J. Pharmacol. Exp. Ther 2003;307:1–8. [PubMed: 12954806]

(7). Seguin B, Uetrecht J. The danger hypothesis applied to idiosyncratic drug reactions. Curr. Opin. Allergy Clin. Immunol 2003;3:235–242. [PubMed: 12865765]

(8). Tirmenstein MA, Nelson SD. Subcellular binding and effects on calcium homeostasis produced by acetaminophen and a nonhepatotoxic regioisomer, 3′-hydroxyacetanilide, in mouse liver. J. Biol. Chem 1989;264:9814–9819. [PubMed: 2524496]

(9). Nelson EB. The pharmacology and toxicology of meta-substituted acetanilide I: Acute toxicity of 3-hydroxyacetanilide in mice. Res. Commun. Chem. Pathol. Pharmacol 1980;28:447–456. [PubMed: 7403659]

(10). Tingle MD, Jewell H, Maggs JL, O'Neill PM, Park BK. The bioactivation of amodiaquine by human polymorphonuclear leucocytes in vitro: chemical mechanisms and the effects of fluorine substitution. Biochem. Pharmacol 1995;50:1113–1119. [PubMed: 7575670]

(11). Bae MA, Rhee H, Song BJ. Troglitazone but not rosiglitazone induces G1 cell cycle arrest and apoptosis in human and rat hepatoma cell lines. Toxicol. Lett 2003;139:67–75. [PubMed: 12595159]

(12). Haskins JR, Rowse P, Rahbari R, de la Iglesia FA. Thiazolidinedione toxicity to isolated hepatocytes revealed by coherent multiprobe fluorescence microscopy and correlated with multiparameter flow cytometry of peripheral leukocytes. Arch. Toxicol 2001;75:425–438. [PubMed: 11693184]

(13). Shishido S, Koga H, Harada M, Kumemura H, Hanada S, Taniguchi E, Kumashiro R, Ohira H, Sato Y, Namba M, Ueno T, Sata M. Hydrogen peroxide overproduction in megamitochondria of troglitazone-treated human hepatocytes. Hepatology 2003;37:136–147. [PubMed: 12500198]

(14). Yamamoto Y, Nakajima M, Yamazaki H, Yokoi T. Cytotoxicity and apoptosis produced by troglitazone in human hepatoma cells. Life Sci 2001;70:471–482. [PubMed: 11798015]

(15). Boelsterli UA, Ho HK, Zhou S, Leow KY. Bioactivation and hepatotoxicity of nitroaromatic drugs. Curr. Drug Metab 2006;7:715–727. [PubMed: 17073576]

(16). Mason RP, Holtzman JL. The mechanism of microsomal and mitochondrial nitroreductase. Electron spin resonance evidence for nitroaromatic free radical intermediates. Biochemistry 1975;14:1626–1632. [PubMed: 164892]

(17). Boelsterli UA. Mechanisms of NSAID-induced hepatotoxicity: Focus on nimesulide. Drug Saf 2002;25:633–648. [PubMed: 12137558]

(18). Berson A, Wolf C, Berger V, Fau D, Chachaty C, Fromenty B, Pessayre D. Generation of free radicals during the reductive metabolism of the nitroaromatic compound, nilutamide. J. Pharmacol. Exp. Ther 1991;257:714–719. [PubMed: 1851835]

(19). Berson A, Wolf C, Chachaty C, Fisch C, Fau D, Eugene D, Loeper J, Gauthier JC, Beaune P, Pompon D. Metabolic activation of the nitroaromatic antiandrogen flutamide by rat and human cytochromes P-450, including forms belonging to the 3A and 1A subfamilies. J. Pharmacol. Exp. Ther 1993;265:366–372. [PubMed: 8386241]

(20). Manso G, Thole Z, Salgueiro E, Revuelta P, Hidalgo A. Spontaneous reporting of hepatotoxicity associated with antiandrogens: data from the Spanish pharmacovigilance system. Pharmacoepidemiol. Drug Saf 2005;253:253–259.

(21). Wu JC, Merlino G, Cveklova K, Mosinger B, Fausto N. Autonomous growth in serum-free medium and production of hepatocellular carcinomas by differentiated hepatocyte lines that overexpress transforming growth factor alpha 1. Cancer Res 1994;54:5964–5973. [PubMed: 7525051]

(22). Gomez-Lechon MJ, Donato MT, Castell JV, Jover R. Human hepatocytes as a tool for studying toxicity and drug metabolism. Curr. Drug Metab 2003;4:292–312. [PubMed: 12871046]

(23). Vermeir M, Annaert P, Mamidi RN, Roymans D, Meuldermans W, Mannens G. Cell-based models to study hepatic drug metabolism and enzyme induction in humans. Exp. Opin. Drug Metab. Toxicol 2005;1:75–90.

(24). Pierce RH, Franklin CC, Campbell JS, Tonge RP, Chen W, Fausto N, Nelson SD, Bruschi SA. Cell culture model for acetaminophen-induced hepatocyte death in vivo. Biochem. Pharmacol 2002;64:413–424. [PubMed: 12147292]

(25). Teeter ME, Baginsky ML, Hatefi Y. Ectopic inhibition of the complexes of the electron transport system by rotenone, piericidin A, demerol and antimycin A. Biochim. Biophys. Acta 1969;172:331–333. [PubMed: 4304726]

(26). Plymate SR, Tennant MK, Culp SH, Woodke L, Marcelli M, Colman I, Nelson PS, Carroll JM, Roberts CT, Ware JL. Androgen receptor (AR) expression in AR-negative prostate cancer cells results in differential effects of DHT and IGF-I on proliferation and AR activity between localized and metastatic tumors. Prostate 2004;61:276–290. [PubMed: 15368471]

(27). York TP, Plymate SR, Nelson PS, Eaves LJ, Webb HD, Ware JL. cDNA microarray analysis identifies genes induced in common by peptide growth factors and androgen in human prostate epithelial cells. Mol. Carcinog 2005;44:242–251. [PubMed: 16240454]

(28). Plumb JA, Milroy R, Kaye SB. Effects of the pH dependence of 3-(4,5-dimethylthiazol-2-yl)-2,5-diphenyl-tetrazolium bromide-formazan absorption on chemosensitivity determined by a novel tetrazolium-based assay. Cancer Res 1989;49:4435–4440. [PubMed: 2743332]

(29). Gentleman RC, Carey VJ, Bates DM, Bolstad B, Dettling M, Dudoit S, Ellis B, Gautier L, Ge Y, Gentry J, Hornik K, Hothorn T, Huber W, Iacus S, Irizarry R, Leisch F, Li C, Maechler M, Rossini AJ, Sawitzki G, Smith C, Smyth G, Tierney L, Yang JY, Zhang J. Bioconductor: Open software development for computational biology and bioinformatics. Genome Biol 2004;5:R80. [PubMed: 15461798]

(30). Bolstad BM, Irizarry RA, Astrand M, Speed TP. A comparison of normalization methods for high density oligonucleotide array data based on variance and bias. Bioinformatics 2003;19:185–193. [PubMed: 12538238]

(31). Wu Z IR, Gentleman RC, Murillo FM, Spencer F. A model based background adjustment for oligonucleotide expression arrays. J. Am. Stat. Assoc 2004;99:909–917.

(32). Smyth GK. Linear models and empirical bayes methods for assessing differential expression in microarray experiments. Stat. Appl. Genet. Mol. Biol 2004;3 Article 3.

(33). Tsai J, Sultana R, Lee Y, Pertea G, Karamycheva S, Antonescu V, Cho J, Parvizi B, Cheung F, Quackenbush J. RESOURCERER: A database for annotating and linking microarray resources within and across species. Genome Biol 2001;2 SOFTWARE0002.

(34). Dennis G, Sherman BT, Hosack DA, Yang J, Gao W, Lane HC, Lempicki RA. DAVID: Database for annotation, visualization, and integrated discovery. Genome Biol 2003;4:P3. [PubMed: 12734009]

(35). Hosack DA, Dennis G, Sherman BT, Lane HC, Lempicki RA. Identifying biological themes within lists of genes with EASE. Genome Biol 2003;4:R70. [PubMed: 14519205]

(36). Birch-Machin, M.; Jackson, S.; Kler, RS.; Turnbull, DM. Study of skeletal muscle mitochondrial dysfunction. In: Hash, L.; Jones, D., editors. Methods in Toxicology. Vol. Vol. 2. Academic Press; San Diego: 1993. p. 51-57.

(37). Easterbrook J, Lu C, Sakai Y, Li AP. Effects of organic solvents on the activities of cytochrome P450 isoforms, UDP-dependent glucuronyl transferase, and phenol sulfotransferase in human hepatocytes. Drug Metab. Dispos 2001;29:141–144. [PubMed: 11159803]

(38). Jeong TC, Jeong HG, Yang KH. Induction of cytochrome P-450 by dimethyl sulfoxide in primary cultures of adult rat hepatocytes. Toxicol. Lett 1992;61:275–281. [PubMed: 1641873]

(39). Pitkanen-Arsiola T, Tillman JE, Gu G, Yuan J, Roberts RL, Wantroba M, Coetzee GA, Cookson MS, Kasper S. Androgen and anti-androgen treatment modulates androgen receptor activity and DJ-1 stability. Prostate 2006;66:1177–1193. [PubMed: 16652386]

(40). Waring JF, Ciurlionis R, Jolly RA, Heindel M, Ulrich RG. Microarray analysis of hepatotoxins in vitro reveals a correlation between gene expression profiles and mechanisms of toxicity. Toxicol. Lett 2001;120:359–368. [PubMed: 11323195]

(41). Bammler T, Beyer RP, Bhattacharya S, Boorman GA, Boyles A, Bradford BU, Bumgarner RE, Bushel PR, Chaturvedi K, Choi D, Cunningham ML, Deng S, Dressman HK, Fannin RD, Farin FM, Freedman JH, Fry RC, Harper A, Humble MC, Hurban P, Kavanagh TJ, Kaufmann WK, Kerr KF, Jing L, Lapidus JA, Lasarev MR, Li J, Li YJ, Lobenhofer EK, Lu X, Malek RL, Milton S,

Nagalla SR, O'Malley JP, Palmer VS, Pattee P, Paules RS, Perou CM, Phillips K, Qin LX, Qiu Y, Quigley SD, Rodland M, Rusyn I, Samson LD, Schwartz DA, Shi Y, Shin JL, Sieber SO, Slifer S, Speer MC, Spencer PS, Sproles DI, Swenberg JA, Suk WA, Sullivan RC, Tian R, Tennant RW, Todd SA, Tucker CJ, Van Houten B, Weis BK, Xuan S, Zarbl H. Standardizing global gene expression analysis between laboratories and across platforms. Nat. Methods 2005;2:351–356. [PubMed: 15846362]

(42). Uetrecht J. Screening for the potential of a drug candidate to cause idiosyncratic drug reactions. Drug DiscoVery Today 2003;8:832–837. [PubMed: 12963319]

(43). Boelsterli UA, Lim PL. Mitochondrial abnormalities—A link to idiosyncratic drug hepatotoxicity? Toxicol. Appl. Pharmacol 2007;220:92–107. [PubMed: 17275868]

(44). Jaeschke H. Are cultured liver cells the right tool to investigate mechanisms of liver disease or hepatotoxicity? Hepatology 2003;38:1053–1055. [PubMed: 14567386]

(45). Fau D, Eugene D, Berson A, Letteron P, Fromenty B, Fisch C, Pessayre D. Toxicity of the antiandrogen flutamide in isolated rat hepatocytes. J. Pharmacol. Exp. Ther 1994;269:954–962. [PubMed: 8014883]

(46). Osburn WO, Wakabayashi N, Misra V, Nilles T, Biswal S, Trush MA, Kensler TW. Nrf2 regulates an adaptive response protecting against oxidative damage following diquatmediated formation of superoxide anion. Arch. Biochem. Biophys 2006;454:7–15. [PubMed: 16962985]

(47). James EA, Gygi SP, Adams ML, Pierce RH, Fausto N, Aebersold RH, Nelson SD, Bruschi SA. Mitochondrial aconitase modification, functional inhibition, and evidence for a supramolecular complex of the TCA cycle by the renal toxicant S-(1,1,2,2-tetrafluoroethyl)-L-cysteine. Biochemistry 2002;41:6789–6797. [PubMed: 12022883]

(48). Hinson JA, Reid AB, McCullough SS, James LP. Acetaminophen-induced hepatotoxicity: Role of metabolic activation, reactive oxygen/nitrogen species, and mitochondrial permeability transition. Drug Metab. Rev 2004;36:805–822. [PubMed: 15554248]

(49). Nelson, SD.; Bruschi, SA. Mechanisms of acetaminophen-induced liver disease. In: Kaplowitz, N., editor. Drug Induced Liver Disease. Marcel Dekker; New York and Basel: 2003. p. 287-325.

(50). Vendemiale G, Grattagliano I, Altomare E, Turturro N, Guerrieri F. Effect of acetaminophen administration on hepatic glutathione compartmentation and mitochondrial energy metabolism in the rat. Biochem. Pharmacol 1996;52:1147–1154. [PubMed: 8937421]

(51). Berson A, Schmets L, Fisch C, Fau D, Wolf C, Fromenty B, Deschamps D, Pessayre D. Inhibition by nilutamide of the mitochondrial respiratory chain and ATP formation. Possible contribution to the adverse effects of this antiandrogen. J. Pharmacol. Exp. Ther 1994;270:167–176. [PubMed: 8035313]

(52). Seo YW, Shin JN, Ko KH, Cha JH, Park JY, Lee BR, Yun CW, Kim YM, Seol DW, Kim DW, Yin XM, Kim TH. The molecular mechanism of Noxa-induced mitochondrial dysfunction in p53-mediated cell death. J. Biol. Chem 2003;278:48292–48299. [PubMed: 14500711]

(53). Er E, Oliver L, Cartron PF, Juin P, Manon S, Vallette FM. Mitochondria as the target of the pro-apoptotic protein Bax. Biochim. Biophys. Acta 2006;1757:1301–1311. [PubMed: 16836974]

(54). da-Silva WS, Gomez-Puyou A, de Gomez-Puyou MT, Moreno-Sanchez R, De Felice FG, de Meis L, Oliveira MF, Galina A. Mitochondrial bound hexokinase activity as a preventive antioxidant defense: Steady-state ADP formation as a regulatory mechanism of membrane potential and reactive oxygen species generation in mitochondria. J. Biol. Chem 2004;279:39846–39855. [PubMed: 15247300]

(55). Zhang DD. Mechanistic studies of the Nrf2-Keap1 signaling pathway. Drug Metab. Rev 2006;38:769–789. [PubMed: 17145701]

(56). Soglia JR, Contillo LG, Kalgutkar AS, Zhao S, Hop CE, Boyd JG, Cole MJ. A semiquantitative method for the determination of reactive metabolite conjugate levels in vitro utilizing liquid chromatography-tandem mass spectrometry and novel quaternary ammonium glutathione analogues. Chem. Res. Toxicol 2006;19:480–490. [PubMed: 16544956]

(57). Tevell A, Lennernas H, Jonsson M, Norlin M, Lennernas B, Bondesson U, Hedeland M. Flutamide metabolism in four different species in vitro and identification of flutamide metabolites in human patient urine by high performance liquid chromatography/tandem mass spectrometry. Drug Metab. Dispos 2006;34:984–992. [PubMed: 16540588]

(58). Kang P, Dalvie D, Smith E, Zhou S. Identification of a novel glutathione conjugate of flutamide in incubations with human liver microsomes. Drug Metab. Dispos 2007;35:1081–1088. [PubMed: 17403914]

(59). Coe KJ, Nelson SD, Ulrich RG, He Y, Dai X, Cheng O, Caguyong M, Roberts CJ, Slatter JG. Profiling the hepatic effects of flutamide in rats: a microarray comparison with classical aryl hydrocarbon receptor ligands and atypical CYP1A inducers. Drug Metab. Dispos 2006;34:1266–1275. [PubMed: 16611858]

(60). Liu Y, Kern JT, Walker JR, Johnson JA, Schultz PG, Luesch H. A genomic screen for activators of the antioxidant response element. Proc. Natl. Acad. Sci. U.S.A 2007;104:5205–5210. [PubMed: 17360324]

(61). Wu CC, Hsu MC, Hsieh CW, Lin JB, Lai PH, Wung BS. Upregulation of heme oxygenase-1 by Epigallocatechin-3-gallate via the phosphatidylinositol 3-kinase/Akt and ERK pathways. Life Sci 2006;78:2889–2897. [PubMed: 16378625]

(62). Isenberg JS, Klaunig JE. Role of the mitochondrial membrane permeability transition (MPT) in rotenone-induced apoptosis in liver cells. Toxicol. Sci 2000;53:340–351. [PubMed: 10696782]

(63). Wallace KB. Doxorubicin-induced cardiac mitochondrionopathy. Pharmacol. Toxicol 2003;93:105–115. [PubMed: 12969434]

(64). Goda R, Nagai D, Akiyama Y, Nishikawa K, Ikemoto I, Aizawa Y, Nagata K, Yamazoe Y. Detection of a new N-oxidized metabolite of flutamide, N-[4-nitro-3-(trifluoromethyl)phenyl]hydroxylamine, in human liver microsomes and urine of prostate cancer patients. Drug Metab. Dispos 2006;34:828–835. [PubMed: 16507648]

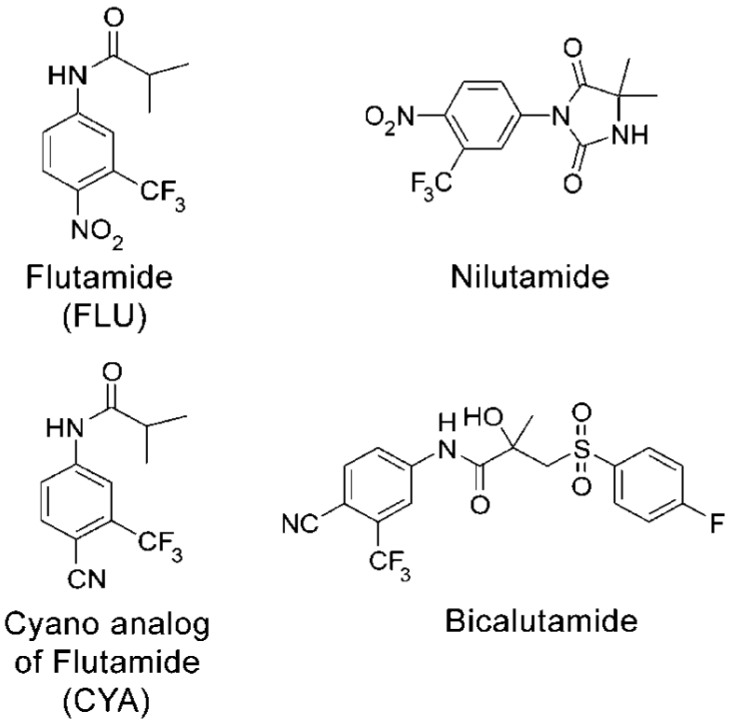

Chart 1.

Structures of FLU, CYA, and its antiandrogen analogues. The structure of FLU, which contains a nitroaromatic group, is compared to two other nonsteriodal antiandrogens, bicalutamide and nilutamide. The nitro to cyano analogue of FLU (CYA) was synthesized to test the contributions of FLU's nitroaromatic group to cytotoxicity

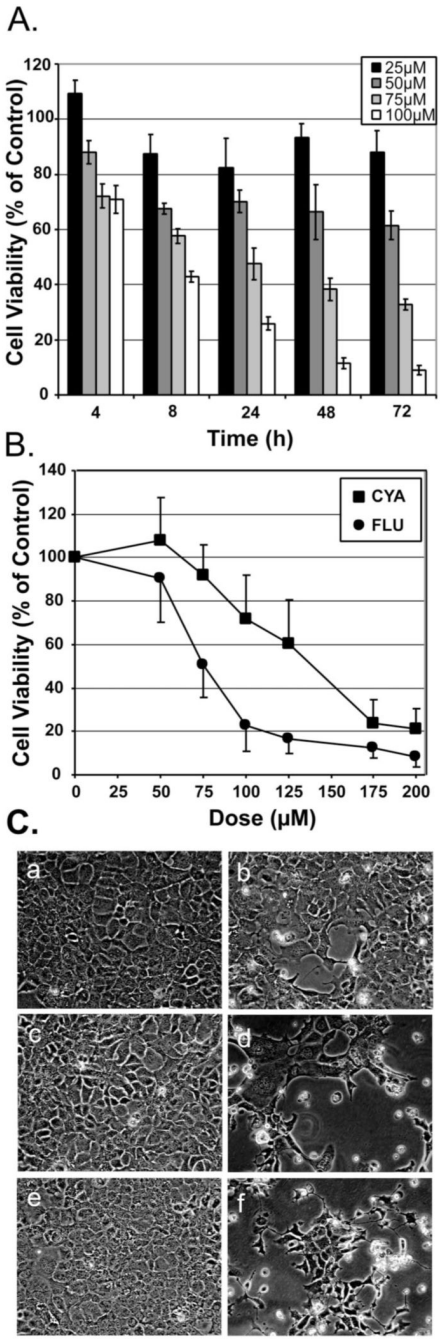

Figure 1.

Comparison of TAMH cell viability between FLU and CYA. (A) MTT cell viability assays were tested at four FLU concentrations (25, 50, 75, and 100 μM) over five time points (4, 8, 24, 48, and 72 h) in the TAMH hepatocyte cell line. Results from an $N = 8$ experiment are expressed as a percentage of cell viability after FLU treatment as compared to DMSO (0.5%) vehicle controls with ± SEM (B) MTT cell viability was compared between CYA and FLU at equimolar concentrations after 24 h. Each data point represents the percent average from three MTT biological replicates, where $N = 24$, as compared to DMSO (1.0%) vehicle controls with ± SEM. An unpaired *t* test, assessing overall type I error by using the Bonferroni correction, was used to compare cell viability at equimolar concentrations of CYA and FLU. A significant

statistical difference of $p < 0.01$ was found at all concentrations except at 50 μM, where the level of significance is $p < 0.05$. (C) Images of the cell monolayer were taken after 24 h treatment of 75 μM CYA (a), 75 μM FLU (b), 100 μM CYA (c), 100 μM FLU (d), 1% DMSO (e), and 200 μM FLU (f) using a Nikon Diaphot 200 light microscope at exposures between 30 and 40 s. White globules are cells detached from the monolayer.

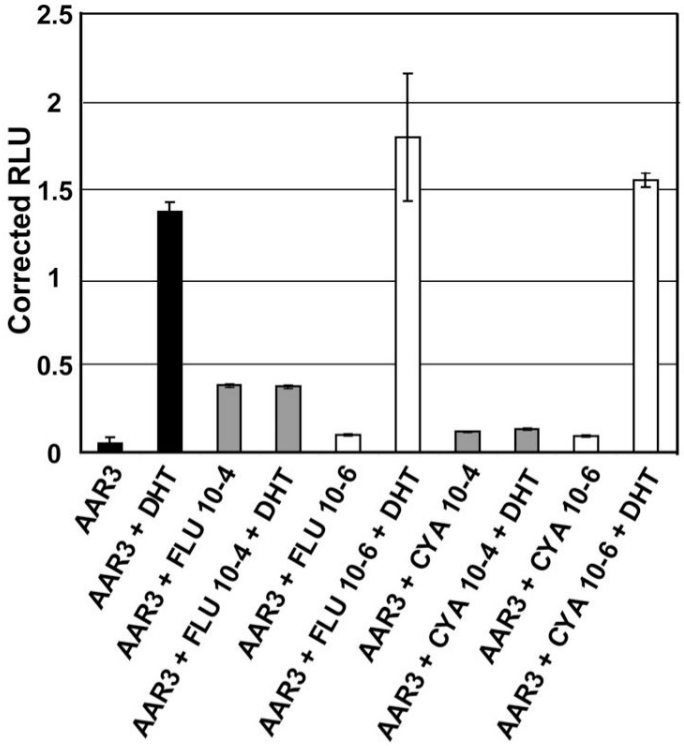

Figure 2.

Antiandrogen activity of FLU as compared to CYA. CYA and FLU at concentrations of 100 (gray bars) and 1 μM (white bars) were assessed for their ability to antagonize 100 pM DHT activation of the AR in M12 AR cells transiently transfected with the luciferase ARE promoter construct AAR3 (black bars) after 24 h of treatment. CYA and FLU were also added in the absence of DHT to test for partial agonist activity. RLU refers to the relative luminescence units, which have been corrected for transfection efficiency.

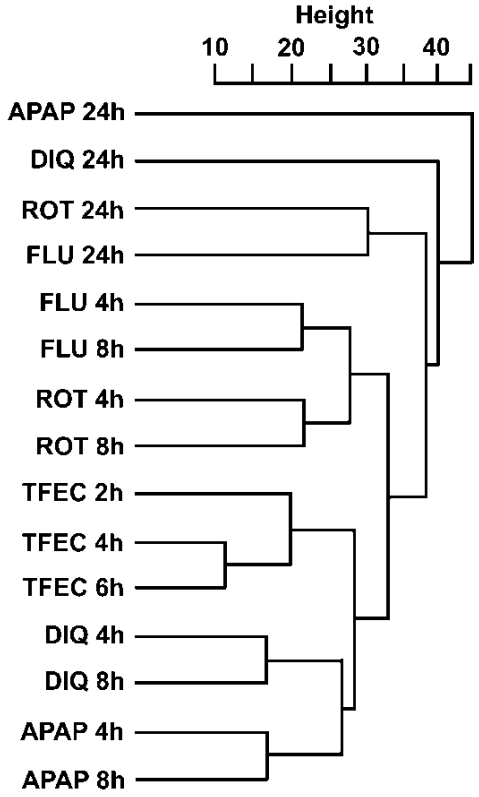

Figure 3.

Dendrogram of FLU toxicogenomic screening analysis. The following compounds, APAP, DIQ, FLU, ROT, and TFEC, were added in the TAMH cell line using each compound's LD_{50} concentration at their final time point. Using Amersham's "Codelink" microarray platform, gene probes with a fold change cutoff of >2 as compared to the vehicle control were extracted (2031 gene probes in all) and used for two-dimensional hierarchical clustering to generate a dendrogram for sample gene response.

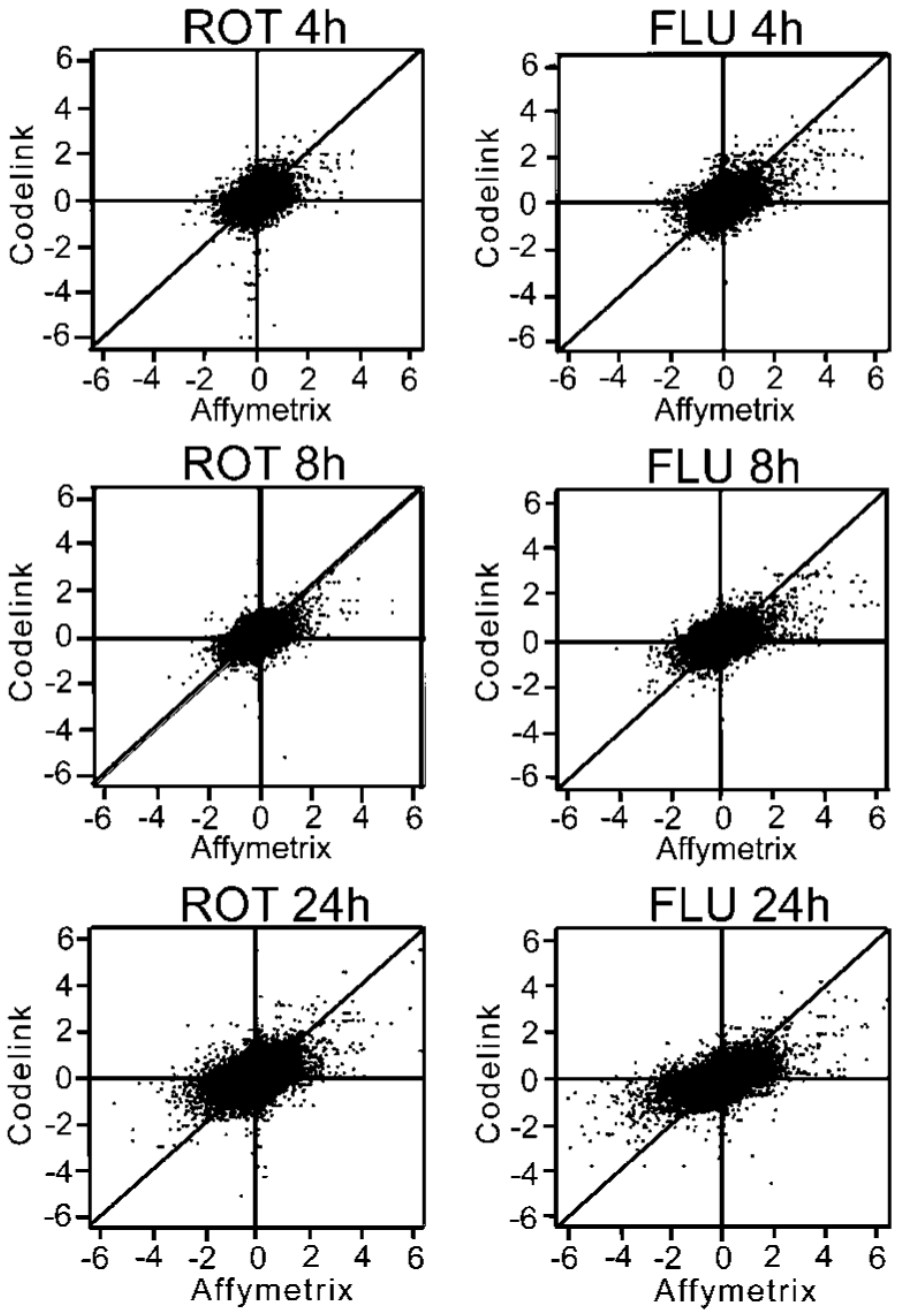

Figure 4.

Codelink and Affymetrix platform comparison using common gene probes between the array studies for FLU and ROT treatments. To discern the variability between the two array studies, using either Amersham's "Codelink" platform or Affymetrix's platform, common gene probes between the two platforms were identified and mapped according to their fold changes after ROT and FLU treatment over 4, 8, and 24 h. The *x*-axis represents the Affymetrix fold change, and the *y*-axis represents the Codelink fold change. Each black dot represents a shared gene probe, and those dots that have a slope of 1 (i.e., that lie along the 45° axis) have identical fold change responses between the two array platforms.

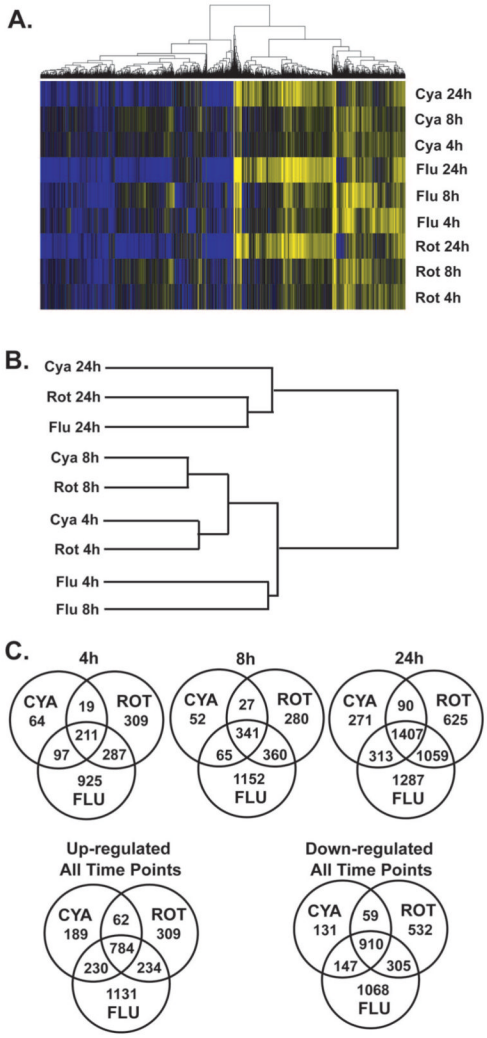

Figure 5.

Array analysis of CYA, FLU, and ROT using the Affymetrix platform. The TAMH cell line was incubated for 4, 8, and 24 h with CYA (75 μM), FLU (75 μM), and ROT (1 μM), and isolated RNA was used for array analysis on the Affymetrix platform. (A) Gene probes that had a fold change cutoff of >2 as compared to DMSO vehicle control (0.15%) were collected (6675 gene probes in total) and used for one-dimensional hierarchical clustering with samples manually ordered. Up- and down-regulated gene probes are represented in yellow and blue, respectively. (B) The gene probes described from panel A were used for two-dimensional hierarchical gene clustering to generate a dendrogram that segregates sample treatment according to their gene expression pattern. (C) Venn diagrams either presented temporally (top) or as a summation of all time points of gene probes up- and down-regulated (bottom) are drawn to show the commonality and exclusivity in the gene expression among the three compounds CYA, FLU, and ROT. Only gene probes with a cutoff of >2 fold change were used for Venn diagram analysis, and their enrichment in each of the various compound gene subsets is numerically associated.

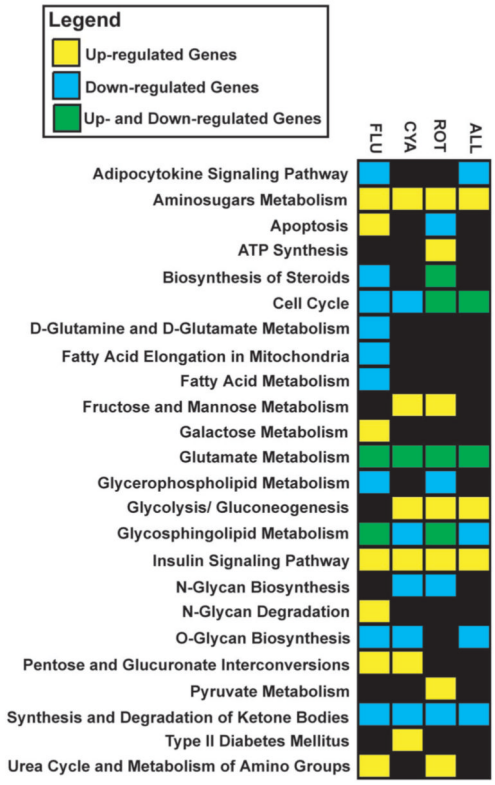

Figure 6.

KEGG pathway analysis of the up- and down-regulated gene probes of the CYA, FLU, and ROT array study. The gene probes from the Venn diagram analysis of Figure 5C (bottom) were assessed using the web-accessible software tool DAVID (34) to identify statistically significant KEGG pathways. Genes regulated for CYA, FLU, ROT, or all three compounds commonly (ALL) identified significant KEGG pathways related to carbohydrate and fatty acid energy metabolism and cell cycle (listed vertically). KEGG pathways found statistically significant using up-regulated, down-regulated, or both up- and down-regulated genes for each compound gene set are represented by orange, cyan, and green boxes, respectively. Nonresponsive pathways for a given compound gene set are blackened.

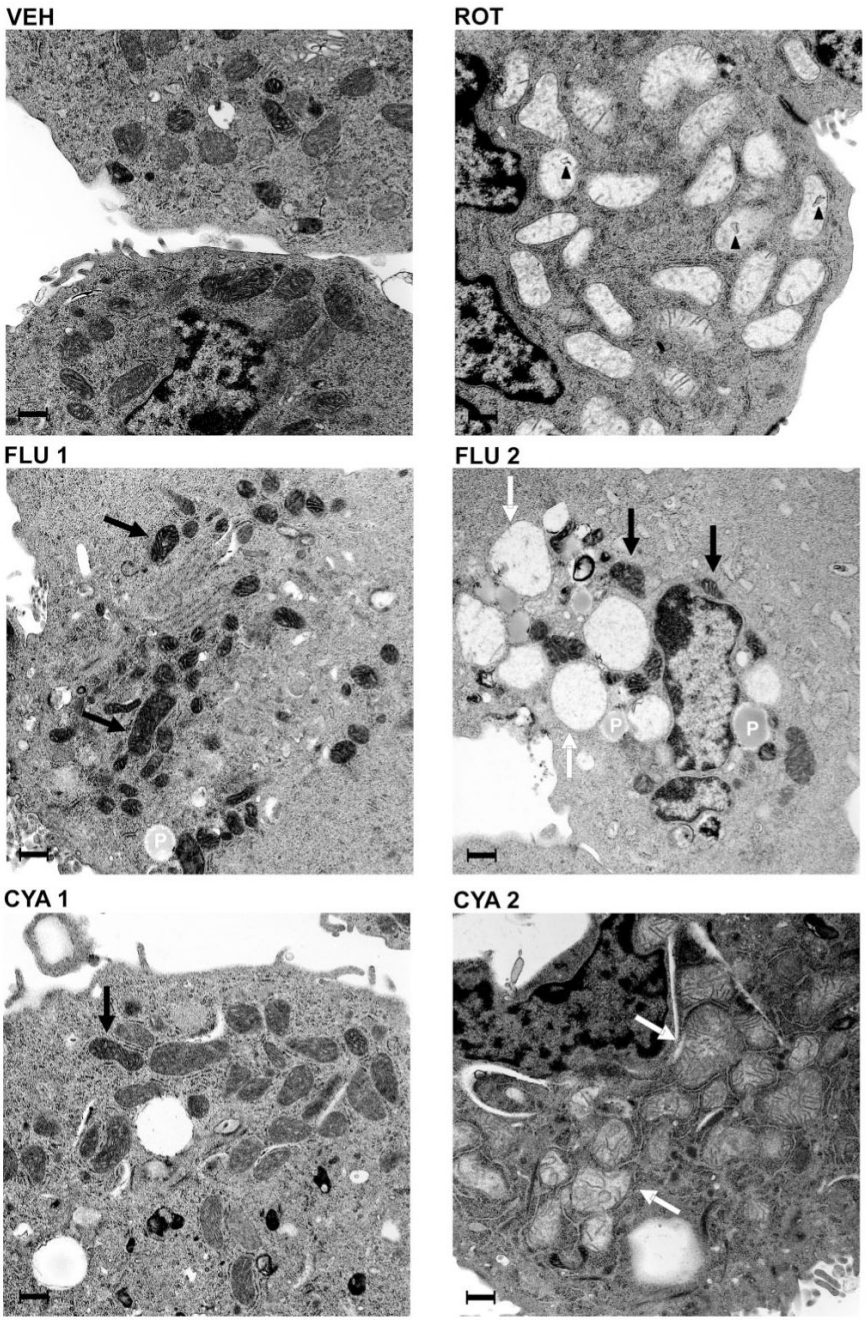

Figure 7.

Electron microscopy analysis after CYA, FLU, and ROT treatments. TAMH cells were incubated for 24 h with DMSO vehicle (0.15%), CYA (75 μM), FLU (75 μM), and ROT (1 μM) before they were collected for electron microscopy analysis. High-powered magnifications of cells laden with mitochondria are pictured with a black reference bar, corresponding to a width of 500 nm. Because of the variable nature of CYA and FLU mitochondrial morphologies, two snapshots were taken for each compound, each depicting a different cell's morphology. Calcium phosphate crystal deposits found in ROT are designated with a black arrowhead. Selected electron dense mitochondria of CYA and FLU are denoted

with a black arrow. Selected swollen mitochondria of CYA and FLU are denoted with a white arrow. Phagolysosomes found in FLU snapshots are designated with a P (in white).

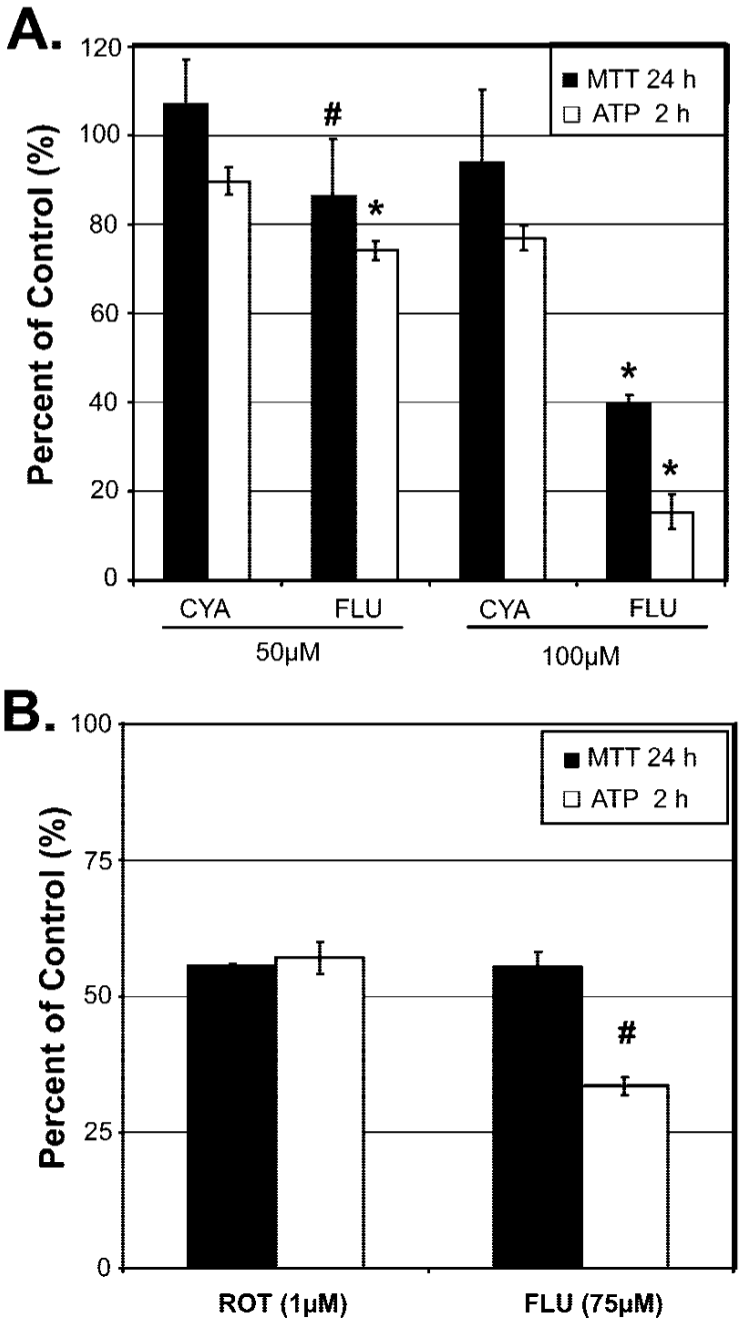

Figure 8.

Comparison of ATP depletion between FLU, CYA, and ROT. (A) Cellular ATP levels were monitored after 2 h of 50 and 100 μM treatments of either FLU or CYA and correlated to a 24 h MTT cell viability assay, where N) 6 for each assay. An average of DMSO (0.5%)-treated cells represents the maximum percent activity of cellular ATP levels and cell viability. An unpaired t test, assessing overall type I error by using the Bonferroni correction, was used to compare FLU and CYA response and showed statistical differences in both MTT and ATP assays (#, $p < 0.05$; *, $p < 0.01$). (B) Using an LD_{50} concentration of ROT (1 μM) and FLU (75 μM), cellular ATP levels were monitored after 2 h, where N) 4. FLU displayed a statistically significant lower ATP level than ROT (#, $p < 0.05$) using an unpaired t test.

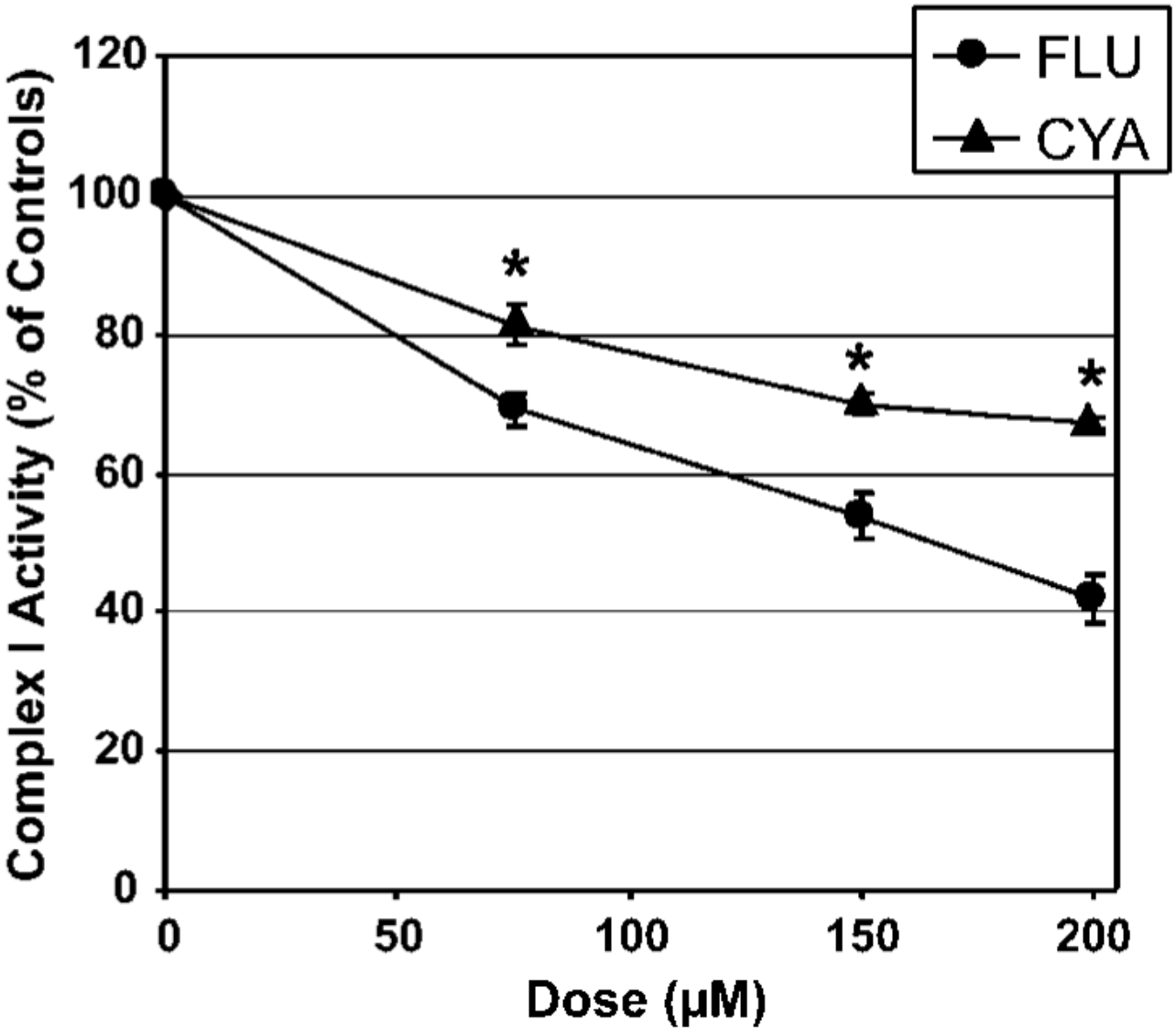

Figure 9.

Complex I inhibition by FLU and CYA. TAMH mitochondrial extracts were tested for complex I activity by spectrally monitoring the depletion of NAD(H) after 3 min at 30 °C in triplicate. Vehicle controls yielded a complex I activity of 153.8 ± 12.6 nmol of NAD(H) depletion/min/mg of mitochondrial protein, which was set as the maximum percent activity. Complex I inhibition by FLU and CYA was tested at 75, 150, and 200 μM and expressed as a percent activity as compared to vehicle controls. FLU caused statistically greater inhibition than CYA at all concentrations (*, $p < 0.01$) using an unpaired *t* test that assessed overall type I error by using the Bonferroni correction. ROT at 1 μM reduces complex I activity to 20.1 ± 2.8 nmol/mg/min, an 87% reduction in activity as compared to vehicle.

Table 1

Selected Regulated Gene Probes[a]

Affymetrix probe ID	accession code	gene symbol	gene name	CYA			ROT			FLU		
				4 h	8 h	24 h	4 h	8 h	24 h	4 h	8 h	24 h
(a) fatty acid metabolism												
1422526_at	BI413218	Acsl1	*acyl-CoA synthetase long-chain family member 1*	−0.7	−0.6	0.6	−0.8	−0.9	−0.4	−0.6	**−1.1**	**−1.1**
1428082_at	AK006541	Acsl5	*acyl-CoA synthetase long-chain family member 5*	0.0	0.0	−0.4	0.0	0.0	−0.6	−0.1	−0.2	**−1.1**
1460409_at	AI987925	Cpt1a	*carnitine palmitoyltransferase 1a, liver*	−0.5	−0.7	−0.7	−0.6	**−1.0**	**−1.0**	−0.5	**−1.2**	**−1.5**
1423109_s_at	AV008091	Slc25a20	*solute carrier family 25 (mitochondrial carnitine/ acylcarnitine translocase), member 20*	−0.2	−0.7	**−1.4**	−0.6	**−1.1**	**−1.7**	−0.5	**−1.3**	**−2.4**
1416772_at	NM_009949	Cpt2	*carnitine palmitoyltransferase 2*	−0.1	−0.7	−0.2	−0.7	−0.7	−0.4	−0.5	**−1.1**	−0.8
1415984_at	NM_007382	Acadm	*acyl-coenzyme A dehydrogenase, medium chain*	−0.1	−0.5	−0.3	−0.3	−0.8	−0.8	0.0	−0.5	**−1.1**
1448987_at	BB728073	Acadl	*acyl-coenzyme A dehydrogenase, long-chain*	−0.2	−0.4	−0.7	−0.1	−0.4	−0.8	−0.1	−0.8	**−1.2**
1448382_at	NM_023737	Ehhadh	*enoyl-coenzyme A, hydratase/3-hydroxyacyl coenzyme A dehydrogenase*	−0.8	−0.3	−0.4	−0.9	−0.4	**−2.0**	−0.5	**−1.0**	**−1.9**
1452173_at	AW107842	Hadha	*hydroxyacyl-coenzyme A dehydrogenase/3-ketoacyl-coenzyme A thiolase/enoyl-coenzyme A hydratase (trifunctional protein), α-subunit*	−0.2	−0.7	−0.6	−0.1	−0.6	−0.7	0.0	−0.7	**−1.1**
1426522_at	BG866501	Hadhb	*hydroxyacyl-coenzyme A dehydrogenase/3-ketoacyl-coenzyme A thiolase/enoyl-coenzyme A hydratase (trifunctional protein), α-subunit*	−0.5	**−1.0**	**−1.0**	−0.7	**−1.4**	**−1.5**	−0.7	**−1.5**	**−1.6**
1419499_at	NM_008149	Gpam	*glycerol-3-phosphate acyltransferase, mitochondrial*	−0.6	−0.5	−0.5	**−1.0**	−0.7	**−1.2**	**−1.1**	**−1.6**	**−1.7**
1417900_a_at	NM_013703	Vldlr	*very low density lipoprotein receptor*	**1.2**	**2.1**	**1.8**	**1.0**	**2.3**	**1.3**	**1.9**	**3.1**	**1.8**
(b) mitochondrial oxidative phosphorylation												
1430149_at	AA060162	Ndufa3	*NADH dehydrogenase (ubiquinone) 1 α-subcomplex, 3*	0.0	0.1	0.4	0.1	0.2	**1.6**	0.0	0.3	**1.9**
1425919_at	BC004633	Ndufa12	*NADH dehydrogenase (ubiquinone) 1 α-subcomplex, 12*	−0.1	0.3	0.9	0.1	0.4	**1.3**	0.0	0.1	0.8
1435934_at	AI643884	Ndufab1	*NADH dehydrogenase (ubiquinone) 1, α/β-subcomplex, 1*	0.1	**1.0**	**1.4**	0.6	**1.2**	**1.0**	0.6	**1.3**	**1.6**
1453565_at	AV221509	Ndufab1	*NADH dehydrogenase (ubiquinone) 1, α/β-subcomplex, 1*	−0.1	**−1.4**	−0.6	0.0	**−1.3**	−0.6	0.0	**−1.4**	−0.6
1423711_at	BC018422	Ndufaf1	*NADH dehydrogenase (ubiquinone) 1 α-subcomplex, assembly factor 1*	0.1	0.0	0.0	**−1.0**	−0.7	−0.2	−0.2	0.0	−0.1
1458404_at	AI604670	Ndufb8	*NADH dehydrogenase (ubiquinone) 1 β-subcomplex 8*	−0.2	**−1.4**	−0.3	−0.2	−0.8	−0.2	−0.2	**−1.7**	−0.8

Affymetrix probe ID	accession code	gene symbol	gene name	CYA			ROT			FLU		
				4 h	8 h	24 h	4 h	8 h	24 h	4 h	8 h	24 h
1430326_s_at	AK003160	Uqcrq	*ubiquinol-cytochrome c reductase, complex III subunit VII*	0.3	0.3	0.9	0.2	0.2	**1.0**	0.1	0.3	**1.1**
1415710_at	BM123013	Cox18	*COX18 cytochrome c oxidase assembly homologue (S. cerevisiae)*	0.1	0.1	0.6	0.0	0.2	0.8	0.0	0.2	**1.2**
1421772_a_at	NM_009187	Cox7a2l	*cytochrome c oxidase subunit VIIa polypeptide 2-like*	0.1	0.1	0.6	0.1	0.2	**1.1**	0.3	0.4	**1.1**
1459884_at	AA190297	Cox7c	*cytochrome c oxidase, subunit VIIc*	0.0	−0.1	0.6	0.4	−0.5	**1.4**	−0.7	0.2	0.9
1438809_at	AI644507	Atp5c1	*ATP synthase, H+ transporting, mitochondrial F1 complex, γ-polypeptide 1*	0.1	0.0	**2.4**	0.2	0.2	**3.5**	0.6	0.2	**3.6**
1459949_at	BI076631	Atp5s	*ATP synthase, H+ transporting, mitochondrial F0 complex, subunit s*	0.1	0.2	**1.0**	0.1	0.2	**1.4**	0.1	0.2	**1.7**
(c) cell stress												
1449363_at	BC019946	Atf3	*activating transcription factor 3*	**1.7**	**1.0**	**1.1**	**1.1**	**1.6**	**2.3**	**3.8**	**2.9**	**2.4**
1449519_at	NM_007836	Gadd45a	*growth arrest and DNA-damage-inducible 45 α*	**2.0**	**1.9**	**2.1**	**1.6**	**2.4**	**2.1**	**3.4**	**3.1**	**3.4**
1416837_at	BC018228	Bax	*Bcl2-associated X protein*	0.1	0.0	0.5	−0.1	0.0	**1.1**	0.0	0.3	**1.2**
1418203_at	NM_021451	Pmaip1	*phorbol-12-myristate-13-acetate-induced protein 1*	0.3	−0.1	0.8	0.7	0.3	**1.2**	**1.1**	0.2	0.9
1449935_a_at	AK004575	Dnaja3	*DnaJ (Hsp40) homologue, subfamily A, member 3*	0.4	0.5	0.9	0.2	0.5	0.8	0.6	0.9	**1.5**
1452262_at	AK003011	Grpel2	*GrpE-like 2, mitochondrial*	0.9	0.6	**1.4**	**1.3**	0.9	**1.7**	**1.4**	**1.4**	**1.8**
1421040_a_at	NM_008182	Gsta2	*glutathione S-transferase, α 2 (Yc2)*	−0.1	0.0	0.0	0.0	0.0	0.1	**1.2**	**4.2**	**4.4**
1426261_s_at	D87867	Ugt1a6a	*UDP glucuronosyltransferase 1 family, polypeptide A6A*	−0.1	0.2	**1.1**	−0.3	−0.3	0.1	0.5	**1.3**	**2.0**
1424296_at	BC019374	Gclc	*glutamate-cysteine ligase, catalytic subunit*	0.2	−0.3	0.8	−0.6	−0.8	0.5	**1.4**	0.6	**1.0**
1448239_at	NM_010442	Hmox1	*heme oxygenase (decycling) 1*	0.7	0.9	0.1	0.4	**1.2**	0.2	**2.8**	**2.3**	0.5
1458703_at	BM212835	Gsr	*glutathione reductase 1*	0.0	0.1	0.0	0.0	0.0	0.0	**1.6**	0.0	0.0
1421557_x_at	NM_019913	Txn2	*thioredoxin 2*	0.1	0.0	0.6	0.0	0.0	0.8	−0.1	0.3	**1.5**
(d) carbohydrate metabolism												
1420901_a_at	NM_010438	Hk1	*hexokinase 1*	0.2	0.1	0.6	0.4	0.2	**1.0**	0.1	0.4	**1.0**
1422612_at	NM_013820	Hk2	*hexokinase 2*	**1.1**	**1.2**	0.7	**1.2**	**1.3**	0.9	**1.4**	**1.8**	**1.4**
1456909_at	BF017016	Gpi1	*glucose phosphate isomerase 1*	0.0	0.1	**1.4**	−0.2	0.0	**1.2**	0.0	0.0	**2.0**
1450269_a_at	NM_008826	Pfkl	*phosphofructokinase, liver, B-type*	−0.1	−0.4	**−1.1**	**−1.0**	**−1.0**	−0.1	0.0	−0.2	−0.4
1433604_x_at	BG065457	Aldoa	*aldolase 1, A isoform*	0.2	−0.1	0.8	−0.3	−0.3	0.8	0.3	0.0	**1.0**
1451194_at	BC024112	Aldob	*aldolase 2, B isoform*	0.0	−0.3	0.0	0.0	−0.3	**−1.6**	0.0	−0.3	**−1.6**
1421258_a_at	NM_013631	Pklr	*pyruvate kinase liver and red blood cell*	0.4	0.2	−0.9	−0.1	0.2	−0.8	−0.1	−0.5	**−2.2**

Affymetrix probe ID	accession code	gene symbol	gene name	CYA			ROT			FLU		
				4 h	8 h	24 h	4 h	8 h	24 h	4 h	8 h	24 h
1417273_at	NM_013743	Pdk4	*pyruvate dehydrogenase kinase, isoenzyme 4*	**−2.1**	**−2.3**	−0.5	**−1.0**	**−2.1**	**−1.3**	0.2	**−2.2**	**−2.2**
1431178_at	BF016392	Aco2	*aconitase 2, mitochondrial*	**−1.1**	**−1.0**	−0.7	**−1.0**	**−1.3**	−0.5	**−1.7**	**−1.7**	−0.8
1452583_s_at	AV307219	Galm	*galactose mutarotase*	0.0	**1.0**	**1.3**	−0.5	0.3	**1.0**	−0.1	**1.3**	**1.3**
1425610_s_at	AF348968	Galnt2	*UDP-N-acetyl-α-D-galactosamine:polypeptide N-acetylgalactosaminyltransferase 2*	−0.2	−0.4	**−1.2**	−0.4	−0.4	**−1.2**	−0.9	−0.8	**−1.6**
1449006_at	NM_013463	Gla	*galactosidase, α*	−0.5	0.8	**1.2**	0.1	**1.2**	**1.3**	−0.2	**1.1**	**1.5**
1449024_a_at	U07631	Hexa	*hexosaminidase A*	0.3	**1.2**	**1.5**	0.6	**1.1**	**1.2**	0.2	**1.3**	**1.4**
1424048_a_at	BC024618	Cyb5r1	*cytochrome b5 reductase 1*	0.8	**1.5**	**1.5**	0.9	**1.5**	**1.1**	0.7	**2.0**	**2.1**

[a]Gene probes selected for their relationship to fatty acid metabolism, oxidative phosphorylation, cell stress, and carbohydrate metabolism are presented as $\log_2$ fold change ratios, where values of ±1, ±2, and ±3 correspond to a fold change of ±2, ±4, and ±8 as compared to DMSO vehicle control. Gene probe responses with a fold change ≥2 are placed in bold.